CHALMERS
UNIVERSITY OF TECHNOLOGY

Mathematical Modeling for Reconfigurable Battery Systems With Parallel-Series Connections

Citation for the original published paper (version of record):
Ouyang, Q., Skegro, A., Hu, L. et al (2026). Mathematical Modeling for Reconfigurable Battery Systems With Parallel-Series Connections. IEEE Transactions on Control Systems Technology, 34(1): 186-202. http://dx.doi.org/10.1109/TCST.2025.3604462

(article starts on next page)

Mathematical Modeling for Reconfigurable Battery Systems With Parallel–Series Connections

Quan Ouyang, *Member, IEEE*, Albert Škegro, *Student Member, IEEE*, Lin Hu, *Member, IEEE*, Weiji Han, *Member, IEEE*, Dezhi Ren, *Student Member, IEEE*, Changyou Geng, *Graduate Student Member, IEEE*, Torsten Wik, *Senior Member, IEEE*, and Changfu Zou, *Senior Member, IEEE*

***Abstract*—Utilizing controllable switches in battery systems can provide flexible and dynamic configurations for batteries at the cell, bank, and pack levels. The reconfigurable battery packs (RBPs) enable optimization of connection configurations with respect to the overall performance, safety, and lifetime. Despite multiple topologies and control strategies previously proposed in the literature, the quantitative analysis and systematic performance evaluation of RBP dynamics remain challenging due to the absence of a mathematical model at the pack level. To bridge this gap, this work introduces a unified modeling framework for various RBPs. We first develop logic gate-based mappings between the operation of batteries and controllable switches, allowing for the isolation or connection of any battery cell or bank. Following this, we develop detailed battery models in state-space form from cells to complete packs. Illustrative and experimental results show that these models are able to accurately and efficiently capture the internal states of RBPs, such as the state-of-charge (SOC), voltage, and current distribution of individual cells under different scenarios. This novel modeling framework and its internal models can significantly simplify the analyses, design, and management of RBPs.**

***Index Terms*—Battery management, battery systems, logic gate, reconfigurable battery packs (RBPs), unified model.**

Received 23 February 2025; revised 4 August 2025; accepted 24 August 2025. Date of publication 8 September 2025; date of current version 30 December 2025. This work was supported in part by the Marie Skłodowska-Curie Actions Postdoctoral Fellowships through the Horizon Europe Programme under Grant 101067291, in part by the Fundamental Research Funds for the Central Universities under Grant NS2024019, in part by Swedish Research Council under Grant 2023-04314, in part by the National Natural Science Funds for Distinguished Young Scholar under Grant 52325211, in part by the Science and Technology Innovation Program of Hunan Province under Grant No. 2024RC4004, and in part by the Open Research Project of Provincial Engineering Research Center for New Energy Vehicle Intelligent Control and Simulation Test Technology of Sichuan under Grant XNYQ2024-006. Recommended by Associate Editor S. Onori. *(Corresponding author: Changfu Zou.)*

Quan Ouyang is with the Department of Electrical Engineering, Chalmers University of Technology, 41296 Gothenburg, Sweden, also with the Provincial Engineering Research Center for New Energy Vehicle Intelligent Control and Simulation Test Technology of Sichuan, Chengdu, China, and also with the College of Automation Engineering, Nanjing University of Aeronautics and Astronautics, Nanjing 210016, China (e-mail: quano@chalmers.se).

Albert Škegro, Torsten Wik, and Changfu Zou are with the Department of Electrical Engineering, Chalmers University of Technology, 41296 Gothenburg, Sweden (e-mail: skegro@chalmers.se; tw@chalmers.se; changfu.zou@chalmers.se).

Lin Hu is with the College of Automotive and Mechanical Engineering, Changsha University of Science and Technology, Changsha 410205, China (e-mail: hulin@csust.edu.cn).

Weiji Han, Dezhi Ren, and Changyou Geng are with China-UK Low Carbon College, Shanghai Jiao Tong University, Shanghai 201306, China (e-mail: w.han@sjtu.edu.cn; dezhi.ren@sjtu.edu.cn; gengchangyou@sjtu.edu.cn).

Digital Object Identifier 10.1109/TCST.2025.3604462

NOMENCLATURE

Abbreviation	Expansion
$B_{i,j}$	Cell j in bank i.
I^b_i	Current of bank i.
I^b	Current vector for all battery banks.
$I^c_{i,j}$	Current of $B_{i,j}$.
I^c_i	Current vector for all cells in bank i.
I^c	Current vector for all cells in the pack.
I^c_M	Maximum allowed cell current.
I^c_m	Minimum allowed cell current.
I^p	Current of the battery pack.
m	Number of cells in each battery bank.
n	Number of banks in the battery pack.
$Q_{i,j}$	Ampere–hour capacity of $B_{i,j}$.
r_{bs}	Contact resistance of the bank-level switch.
r_{cs}	Contact resistance of the cell-level switch.
$r_{i,j}$	Internal resistance of $B_{i,j}$.
$S^b_{i,1}$, $S^b_{i,2}$, and $S^b_{i,3}$	Bank-level switches.
$S^c_{i,j}$	Cell-level switch.
$\mathrm{SOC}_{i,j}$	State-of-charge (SOC) of cell $B_{i,j}$.
$\mathrm{SOC_i}$	SOC vector for all cells in bank i.
T	Sampling period.
u^b_i	Binary operating state of bank i.
$u^c_{i,j}$	Binary operating state of $B_{i,j}$.
U^b and U^c	Input matrices of the RBP model.
V^b_i	Terminal voltage of bank i.
V^b	Terminal voltage vector for all banks.
$V^c_{i,j}$	Terminal voltage of $B_{i,j}$.
V^c_i	Terminal voltage vector for cells in bank i.
V^c_M	Maximum allowed cell voltage.
V^c_m	Minimum allowed cell voltage.
$V^o_{i,j}$	Open-circuit voltage (OCV) of $B_{i,j}$.
V^o_i	OCV vector for all cells in bank i.
V^o	OCV vector for all cells in the pack.
V^p	Terminal voltage of the battery pack.
x	State vector of the RBP model.
y	Output vector of the RBP model.
η	Coulombic efficiency.

I. INTRODUCTION

THE rapid development of electric vehicles (EVs) and energy storage systems (ESSs) has placed lithium-ion

(Li-ion) batteries at the forefront of research and innovation. Due to its inherent electrochemical characteristics, the voltage of a single Li-ion battery cell typically ranges from 2.0 to 4.2 V. To meet the high-current and high-voltage demands in EV and ESS applications, hundreds or even thousands of cells are commonly interconnected in both series and parallel within a battery pack. The parallel–series connection is among the most prevalent configurations, in which a certain number of battery cells are arranged in parallel to form battery banks, and these banks are then connected in series to construct a large battery pack [1], [2], [3]. However, cell imbalances arising from inhomogeneous conditions and manufacturing variations result in the battery pack's performance being limited by its weakest cell, rendering a significant portion of the battery pack's capacity severely underutilized.

To address battery imbalances, numerous cell equalization systems have been developed, which can be broadly categorized into passive and active types [4]. Passive cell equalization systems utilize shunt resistors to dissipate the excess energy of higher charged cells, thereby aligning them with lower charged ones [5]. In contrast, active equalization systems transfer and coordinate energy among different cells through external equalizers, such as switched transformers and converters. Compared with their passive counterparts, active equalization systems can significantly improve the energy efficiency and balancing speed of battery packs [6], [7].

Despite these advances, traditional equalizer-based systems equipped in battery packs are limited by fixed pack configurations and are generally focused on balancing SOC. However, it is equally or even more important to balance the temperature and lifetime of different battery cells and to enhance the overall system's reliability and robustness. This underscores the necessity for flexible configurations in more advanced battery management systems (BMSs).

To have more connection flexibility in battery management, reconfigurable battery packs (RBPs) have emerged as a concept enabling dynamic reconfiguration at cell, bank, and/or pack levels [8], [9]. Typical RBPs incorporate a series of controllable switches into the conventional battery pack, allowing to bypass any selected cells or banks. The dynamic reconfiguration capability confers multiple advantages, including enhanced fault tolerance, improved SOC and temperature uniformity, extended energy delivery, and better coordination of cells with heterogeneous ages and chemistries [10].

Existing research on RBPs has mainly focused on developing the hardware infrastructure, particularly exploring diverse switch connection topologies [11], [12], [13], [14]. For example, Han et al. [10] provided a comprehensive summary of various reconfigurable battery topologies that employ between one and six switches per battery cell. Despite the enhanced system flexibility, the cooperative and optimal control of a large number of switches remains a significant challenge in the implementation of dynamic reconfiguration in battery systems. Correspondingly, a few recent attempts have been made to advance the design of configuration control algorithms, such as the flexible path planning-based reconfiguration strategy [14], dual-scale hierarchical equalization scheme [15], and fast battery balance method [16].

In contrast to these preliminary achievements in hardware structures and control algorithms, to the best of the authors' knowledge, no studies have been conducted on establishing mathematical models of RBPs at the pack level. Yet, such models are indispensable for quantitative analysis, performance evaluation, design optimization, and advanced management of RBPs. The closest studies address the modeling of battery packs with fixed configurations, as seen in [17] and [18]. Moreover, for a battery pack with parallel–series connections, several reconfiguration topologies have been proposed, as demonstrated in [11], [12], [13], and [14]. Although these RBP designs offer similar functionalities, they differ in their control variables, primarily due to varying numbers of switches per cell or switch configurations.

Given the diversity in switch configurations and control variables across different RBPs, creating individual models for each design is inefficient and time-consuming. This raises a key research question: How can we develop a unified mathematical model for a wide range of RBP topologies? Solving this problem would streamline model development, improve the analytical consistency, and support scalable deployment of RBPs.

To bridge the identified research gap, this article develops a novel and unified modeling framework for RBPs. Logic gates are basic components of integrated circuits and are commonly used in combination to execute complex logic operations [19]. These components find extensive applications across fields, such as computer hardware [20] and control systems [21], due to their excellent real-time performance and high level of integration. Given their versatility and efficiency in various fields, we introduce logic gates into the field of battery research and establish a set of logic gate-based mappings for three typical RBPs. These mappings enable battery-focused modeling that provides substantial advantages for control-oriented applications compared with conventional switch-based modeling. Following this, we develop unified mathematical models to describe the dynamics of RBPs, encompassing scales from individual cells to complete packs. These models, validated across different scenarios, demonstrate high accuracy, computational efficiency, and adaptability for modeling RBPs of diverse topologies.

II. Overview of RBPs With Parallel–Series Connection

Parallel–series connection is commonly employed in battery packs to meet the high current and voltage requirements of various loads [2]. As illustrated in Fig. 1(a), in a traditional battery pack composed of $m \times n$ battery cells, m cells, labeled as $B_{i,1}, \ldots, B_{i,j}, \ldots, B_{i,m}$ $(1 \le i \le n)$, are connected in parallel in the battery bank i. Subsequently, n banks are connected in series to constitute the battery pack. To transform a traditional battery pack into an RBP, multiple controllable switches are incorporated, enabling the selective bypassing of individual battery cells or entire banks from the electrical circuit. While a comprehensive review of RBPs is available in [10], five

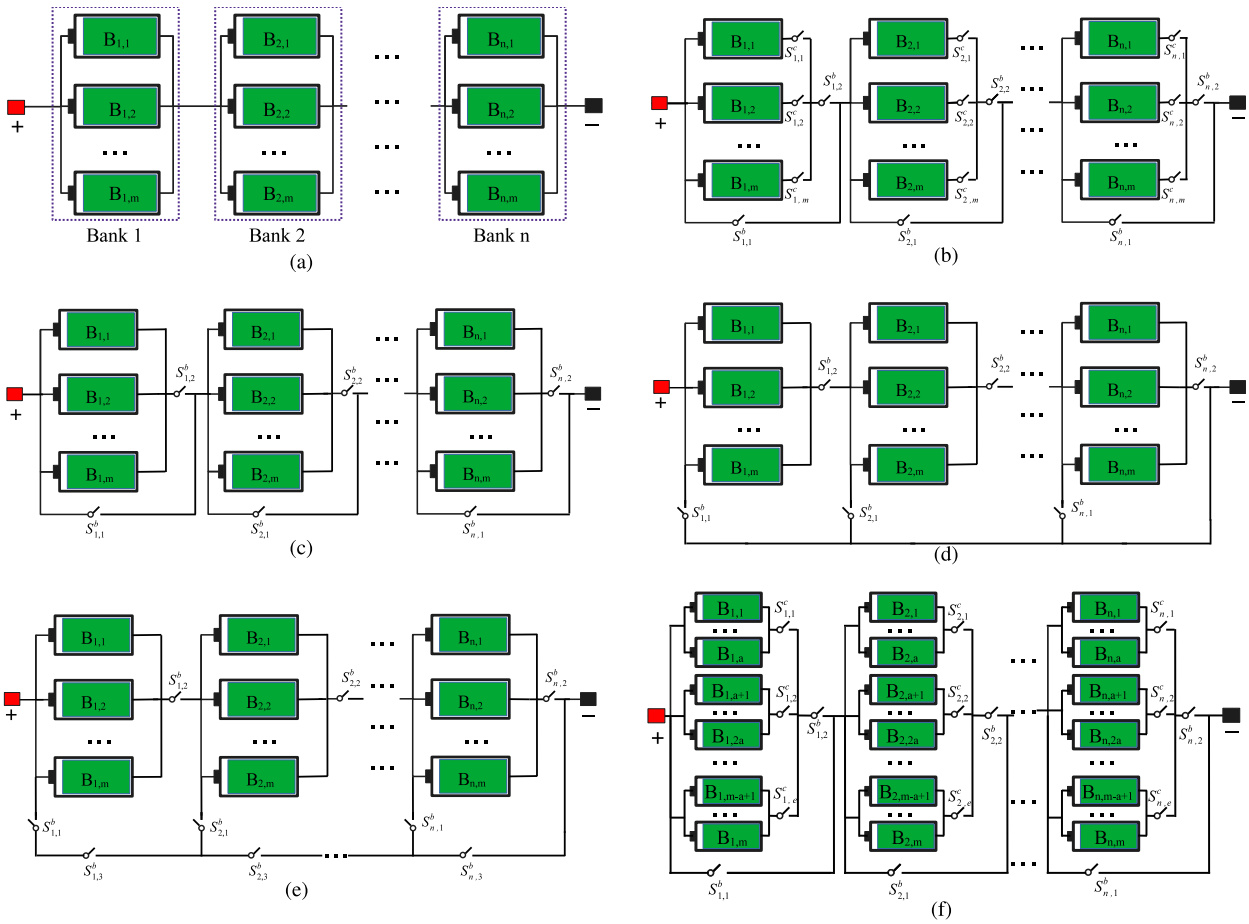

Fig. 1. (a) Traditional battery pack. RBPs with (b) Topology 1 [11], (c) Topology 2 [12], (d) Topology 3 [13], (e) Topology 4 [14], and (f) Topology 5.

typical topologies for RBPs are specified and discussed in this section.

1) *Topology 1 [11]:* As illustrated in Fig. 1(b), each battery bank i is equipped with two bank-level switches, labeled as $S^b_{i,1}$ and $S^b_{i,2}$. Within bank i, each battery cell $B_{i,j}$ $(1 \le j \le m)$ is connected to one cell-level switch $S^c_{i,j}$. By coordinated control of these switches, any cell or bank can be flexibly and dynamically isolated from or connected to the electrical circuit.
2) *Topology 2 [12]:* This configuration maintains the same bank-level switch deployment as Topology 1 [see Fig. 1(c)]. However, unlike Topology 1, each battery bank i is treated as a single large-capacity battery cell, and cell $B_{i,j}$ within bank i cannot be individually bypassed.
3) *Topology 3 [13]:* Each battery bank i is equipped with two bank-level switches $S^b_{i,1}$ and $S^b_{i,2}$, but their connection structure differs from that of Topology 2 [see Fig. 1(d)]. Similar to Topology 2, this configuration does not allow for cell-level isolation within the banks.
4) *Topology 4 [14]:* Each battery bank i is equipped with three bank-level switches [see Fig. 1(e)], denoted by $S^b_{i,1}$, $S^b_{i,2}$, and $S^b_{i,3}$. This topology, as an extension of Topology 3, integrates an additional (redundant) switch for each battery bank, thereby enhancing the overall reliability and safety of the battery pack.

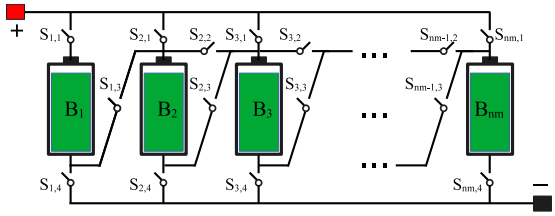

Fig. 2. Illustrative topology of RBPs allowing arbitrary connections of battery cells in the electrical circuit, including series, parallel, and bypass configurations [22].

5) *Topology 5:* Each set of a cells connected in parallel is equipped with one cell-level switch [see Fig. 1(f)]. In contrast to nm cell-level switches required in Topology 1, Topology 5 reduces this number to nm/a. This design effectively balances the advantages of Topologies 1 and 2 by enabling the isolation of groups of parallel cells while significantly reducing the total number of switches required.

Remark 1: The RBPs that allow arbitrary connections of cells in series, parallel, and bypassed configurations, such as the one illustrated in Fig. 2, are not considered in this work. This topology and similar kinds require a substantial number of switches, resulting in prohibitively high hardware costs. Moreover, such configurations can significantly alter

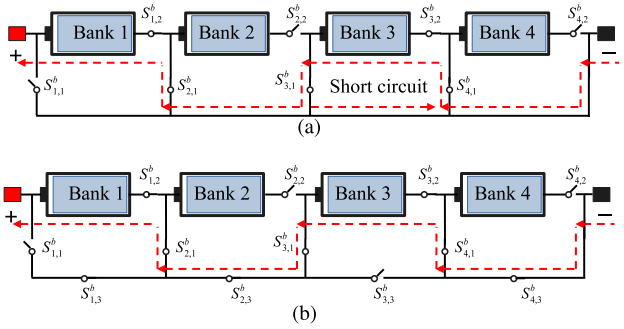

Fig. 3. Operation examples of RBPs with (a) Topology 3 and (b) Topology 4.

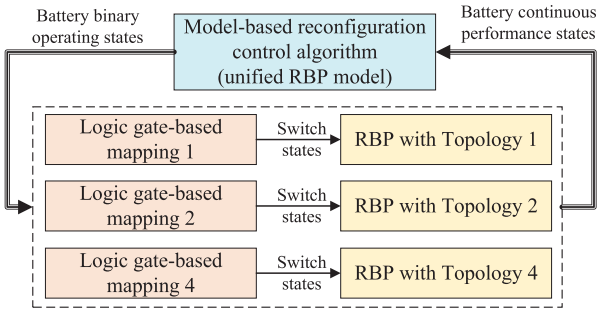

Fig. 4. Model-based control framework for RBPs.

the traditional parallel–series connection structure of battery packs, dramatically increasing system complexity and potentially compromising overall reliability and safety.

It is important to note that in Topology 3, certain switch configurations can lead to the inadvertent short-circuiting of some battery banks and their internal cells. Considering an RBP consisting of four banks [see Fig. 3(a)], a short circuit occurs in bank 3 if banks 2 and 4 are bypassed while bank 3 remains connected. Topology 4 resolves this by adding switches $S^b_{i,3}(1 \le i \le n)$. Topology 4 resolves this by introducing switches $S^b_{i,3}$ $(1 \le i \le n)$, allowing the short circuit to be avoided by disconnecting switch $S^b_{3,3}$ [see Fig. 3(b)].

Due to this inherent risk of short circuits, Topology 3 is excluded from further analysis in this work. Furthermore, for the RBP with Topology 5, users typically treat each set of a battery cells as one large cell with a large capacity and are primarily interested in understanding the dynamics of the single large-capacity cell. Based on this consideration, its dynamics become analogous to those of Topology 1. Hence, this work focuses exclusively on analyzing the RBPs with Topologies 1, 2, and 4.

III. Logic Gates Mapping Operations From Batteries to Switches

While the potential advantages of dynamic reconfiguration in battery packs are significant, experimentally validating these advantages across various scenarios can be resource-intensive and time-consuming. To address this challenge, we turn to mathematical modeling as a powerful and efficient alternative. Mathematical models enable the state evolution of all battery cells in an RBP to be simulated in a cost-effective, rapid, and comprehensive manner. Such models can facilitate quantitative analysis and systematic performance evaluation of RBPs, thereby obviating the need for extensive and complex experimental tests. As a result, significant savings in time, costs, and energy can be achieved. Furthermore, the use of simulations allows for the exploration of a wide range of conditions and scenarios, enhancing the robustness and reliability of the performance assessments.

A. Motivation for Battery-Focused Modeling

The reconfiguration of RBPs, as illustrated in Fig. 1, is achieved through the modulation of controllable switches' operating states. Each cell can be either connected to or bypassed from the electrical circuit, with these states denoted as ON and OFF, respectively. The operating states of controllable switches determine the connection states of the battery cells. These binary states of individual switches serve as the ultimate control variables of RBPs. The number of switches in RBPs varies depending on the specific topology employed. For RBPs composed of nm cells, Topologies 1, 2, and 4 incorporate $nm + 2n$, $2n$, and $3n$ switches, respectively.

A straightforward approach for RBP modeling and model-based management is to consider each switch's operating state as a control variable. However, there are two significant pitfalls to this switch-focused modeling. First, the control objectives of a BMS typically include optimizing battery performance (e.g., with respect to fast charging and cell balancing), lifetime, and safety. Explicitly considering both battery and switch states in a mathematical formulation results in a high-dimensional and complex problem. Specifically, for vehicle or utility-scale battery systems, this approach involves numerous state and control variables, subject to a considerable amount of constraints imposed on these variables. The second pitfall is that given each topology has a unique number or positioning of switches, the switch-focused modeling approach will lead to distinct model formulations for RBPs of different topologies. This implies that mathematical models must be meticulously developed for each individual RBP on a case-by-case basis. While this process requires considerable time and resources, the obtained individual models complicate subsequent model-based analyses, designs, and management of various RBPs.

In contrast, battery-focused modeling offers a fundamentally superior approach that overcomes the limitations of switch-focused modeling. With the battery-focused modeling approach, we only need to consider battery states, including binary operating states and continuous performance states, such as SOC and state of health (SOH) of battery cells. Consequently, the model's dimensionality and complexity can be significantly reduced, leading to lower computational resource consumption and shorter development time. These advantages make battery-focused modeling particularly suitable for large-scale battery packs with hundreds of cells in EVs and ESSs. Moreover, despite variations across different RBPs concerning the number or positioning of switches, the set of operating states remains consistent among these battery systems. In other words, for the configuration control of various RBPs, as illustrated in Fig. 4, the control inputs and state variables

embedded in state-space RBP models will be identical. This uniformity paves the way for the development of a unified model applicable to all considered RBPs.

B. Logic Gate-Based Mappings

Binary variables u_i^b and $u_{i,j}^c$ are used to denote the operating states of battery bank i and its constituent battery cell j, respectively. Specifically, the binary variable being 1 indicates that the corresponding unit, namely a bank or a cell, is connected to the electrical circuit, and 0 indicates disconnection from the circuit. Furthermore, binary variables S^b and S^c are employed to define the operating states of bank-level and cell-level switches, respectively. A value of $S = 1$ denotes that the switch is in the closed position (i.e., "ON" state), while $S = 0$ corresponds to the open position (i.e., "OFF" state).

Logic gates are the fundamental components of digital circuits, responsible for executing elementary Boolean operations, such as conjunction (AND), disjunction (OR), and negation (NOT). Each gate processes one or more binary inputs and generates a single binary output based on a predefined logical function. For instance, an AND gate outputs 1 (high signal) only when all its inputs are 1, while an OR gate outputs 1 if at least one input is 1. A NOT gate inverts the input, outputting 1 for an input of 0 and 0 for an input of 1. Since u and S are the binary variables, logic gates are well-suited for mapping their relationships. Hence, to enable the development of a unified model for various RBP topologies within the battery-focused modeling framework, this section introduces a set of logic gates designed to map battery operations to switch configurations. Each logic gate is specifically tailored to accommodate the unique topology of a particular RBP configuration.

1) Logic Gates for RBPs With Topology 1: As illustrated in Fig. 1(b), the connection or bypass of battery bank i can be achieved through the joint operation of its associated bank-level switches, i.e., $\{S_{i,1}^b, S_{i,2}^b\}$. To bypass battery bank i, switches are set as $S_{i,1}^b = 1$ and $S_{i,2}^b = 0$. At the cell level, the switch $S_{i,j}^c$ determines the connection or isolation of the battery cell $B_{i,j}$ to the electrical circuit. Based on these specifications, the logical relationship between battery operations and switch operations at time step k in this topology can be expressed as follows:

$$S_{i,1}^b(k) = \overline{u_i^b(k)} \tag{1a}$$

$$S_{i,2}^b(k) = u_i^b(k) \tag{1b}$$

$$S_{i,j}^c(k) = u_{i,j}^c(k) \tag{1c}$$

where $\overline{u_i^b}$ denotes the logical NOT operator on u_i^b. Consequently, the logical relationship between battery operations (inputs) and switch operations (outputs) can be represented by the logic gates illustrated in Fig. 5(a).

2) Logic Gates for RBPs in Topology 2: As illustrated in Fig. 1(c), this topology exclusively employs bank-level switches with $S_{i,1}^b$ and $S_{i,2}^b$ controlling each battery bank i. The bank-level operations in this topology are identical to those in Topology 1. Specifically, when $S_{i,1}^b = 0$ and $S_{i,2}^b = 1$, battery bank i is connected to the electrical circuit, corresponding to $u_i^b = 1$. When $S_{i,1}^b = 1$ and $S_{i,2}^b = 0$, the bank is bypassed, namely $u_i^b = 0$. Consequently, the logical relationship between battery operations and switch states is mathematically identical to that described by (1a) and (1b). The corresponding logic gate representation is depicted in Fig. 5(b).

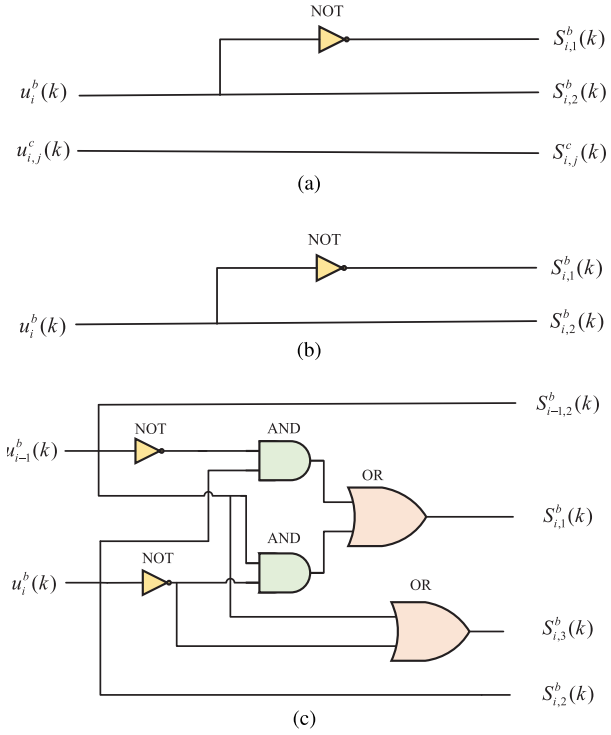

Fig. 5. Logic gates for (a) Topology 1, (b) Topology 2, and (c) Topology 4.

3) Logic Gates for RBPs in Topology 4: As illustrated in Fig. 1(e), switch $S_{i,2}^b$ must be set to 0 when battery bank i requires bypassing (i.e., $u_i^b = 0$). However, the state of $S_{i,1}^b$ cannot be determined solely by u_i^b and must consider the operating states of both battery banks $i-1$ and i. The operating states of battery banks $i-1$ and i present four distinct combinations, as illustrated in Fig. 6. When both banks are simultaneously connected or bypassed, $S_{i,1}^b$ should be OFF, namely, $S_{i,1}^b = 0$. For the other two scenarios, in which only the bank $i-1$ or i is connected, $S_{i,1}^b$ must be turned on, namely, $S_{i,1}^b = 1$.

Based on the preceding analysis, the states of switches $S_{i,1}^b$ and $S_{i,2}^b$ can be modeled by the following logic expressions with respect to u_i^b and u_{i-1}^b

$$S_{i,1}^b(k) = u_{i-1}^b(k)\,\overline{u_i^b(k)} + \overline{u_{i-1}^b(k)}\,u_i^b(k) \tag{2a}$$

$$S_{i,2}^b(k) = u_i^b(k). \tag{2b}$$

The switch $S_{i,3}^b$ must be turned-off when both $S_{i,1}^b$ and $S_{i,2}^b$ are on simultaneously to avoid short-circuiting of battery bank i. When bank i needs to be bypassed, $S_{i,3}^b$ should be turned-on to maintain the continuity of the electrical circuit, as shown in Fig. 6(c) and (d). For the scenario depicted in Fig. 6(a), $S_{i,3}^b$ can be either ON or OFF. To simplify the logical relationship, we define it to be on in this work. Consequently, the control logic for $S_{i,3}^b$ in Topology 4 can be expressed as follows:

$$S_{i,3}^b(k) = \overline{S_{i,1}^b(k)\,S_{i,2}^b(k)} = u_{i-1}^b(k) + \overline{u_i^b(k)}. \tag{3}$$

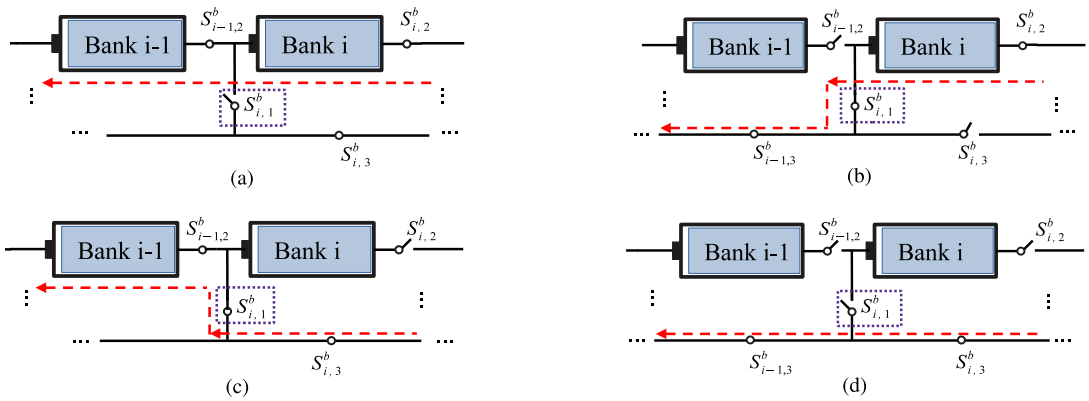

Fig. 6. Switch's states for various connection scenarios of battery banks i and $i+1$. (a) Both banks are connected. (b) Bank $i-1$ is bypassed while Bank i is connected. (c) Bank $i-1$ is connected while Bank i is bypassed. (d) Both banks are bypassed.

It is important to note that in (2) and (3), u_0^b should always be set as 1. The logical relationships described by these equations can be represented by the logic gate configuration illustrated in Fig. 5(c).

4) Virtual Switches to Facilitate Unified Modeling: Unlike Topology 1, RBPs in Topologies 2 and 4 lack cell-level switches, resulting in discrepancies in the number of switches across the three topologies. To facilitate unified modeling at the battery cell level, we introduce virtual cell-level switches $S_{i,j}^c$ to Topologies 2 and 4. These virtual switches are defined to be permanently in the closed position, expressed as follows:

$$S_{i,j}^c(k) = u_{i,j}^c(k) = 1, \quad \forall k. \tag{4}$$

Namely, each battery cell $B_{i,j}$ in Topologies 2 and 4 is conceptually connected to a closed virtual switch.

Another advantage of introducing virtual switches and defining $S_{i,j}^c$ and $u_{i,j}^c$ as in (4) is that even when users specify the disconnection of a particular battery cell $B_{i,j}$ in Topologies 2 and 4, the model will automatically convert this input to $u_{i,j}^c = 1$. This approach ensures that the inherent hardware constraints of Topologies 2 and 4 are consistently respected in the model.

5) Benefits of Using Logic Gate-Based Mappings: In addition to facilitating battery-focused model development, the use of logic gates can bring about a set of other benefits for the management and control of RBPs, as noted in the following.

Remark 2: After establishing the logic gate-based mappings from battery operations to switch operations, the battery binary operating states can be used as model inputs, replacing the actual control inputs, i.e., the switch operating states on the cell and bank levels. This implies that in the battery-focused RBP model, only batteries need to be considered, with no need to incorporate switch states. As a result, the number of control inputs is reduced from $nm+2n$, $2n$, and $3n$ to $nm+n$, n, and n for Topologies 1, 2, and 4, respectively, thereby lowering model dimensionality and complexity. Although the logic gate-based mappings differ among these topologies, they are not required in the subsequently developed battery-focused mathematical model and introduce no additional computational cost. In practical implementations, these mappings can be realized using integrated circuits, such as field-programmable gate arrays (FPGAs).

Remark 3: These logic gates naturally impose hard constraints on switching operations, leading to grouped and coordinated control of switches. This innovative approach can significantly reduce the risks of false control coordination and time delays in the operation of individual switches, which would otherwise undermine the safety, reliability, and performance of RBPs. For example, the switches $S_{i,1}^b$ and $S_{i,2}^b$ in Topology 2 must not be closed simultaneously to avoid short circuits of battery bank i. Through (1a) and (1b), such a constraint is inherently satisfied.

IV. Unified Mathematical Model for RBPs

Building upon the logic gate-based mappings established in Section III, we now develop a unified mathematical model applicable to all considered RBP topologies. This model is constructed hierarchically, starting from individual cells and progressing through battery banks to encompass the entire battery pack. For the unified model, we define the operating states of individual cells and banks, i.e., $u_{i,j}^c$ and u_i^b for $1 \le i \le n$ and $1 \le j \le m$, as its input.

A. Battery Cell Model

The dynamics of any battery cell $B_{i,j}$ within the RBP can be approximately governed by a Rint model [23]. This model offers an optimal balance between computational complexity and model accuracy, particularly for pack-level simulations and predictions for battery behavior. The Rint model is composed of a voltage source representing the OCV, denoted by $V_{i,j}^o$, and a resistor characterizing the internal resistance, defined as $r_{i,j}$. Within this model, the dynamics of $B_{i,j}$ in the RBP are described by

$$\mathrm{SOC}_{i,j}(k+1) = \mathrm{SOC}_{i,j}(k) - \frac{\eta T}{Q_{i,j}} I_{i,j}^c(k) \tag{5a}$$

$$V_{i,j}^c(k) = V_{i,j}^o(k) - r_{i,j}(k)\, I_{i,j}^c(k) \tag{5b}$$

where the state variable $\mathrm{SOC}_{i,j}$ represents the SOC of $B_{i,j}$. The variables $V_{i,j}^c$ and $I_{i,j}^c$ denote the cell's terminal voltage and current, respectively. The parameters η, $Q_{i,j}$, and T indicate

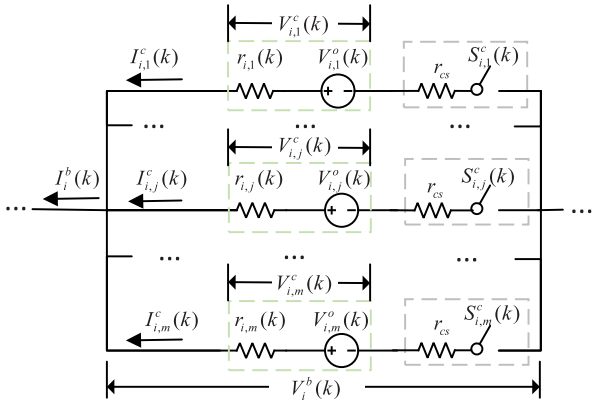

Fig. 7. Equivalent circuit model of the battery bank i with cell-level switches.

the coulombic efficiency, cell capacity, and sampling period for discretization, respectively. We define $I^c_{i,j} > 0$ when the battery cell is discharging and $I^c_{i,j} < 0$ when charging. As shown in (5), the OCV and internal resistance primarily determine the cell's terminal voltage, while the initial SOC and capacity influence the SOC dynamics. The parameterization of battery electrical models has been extensively studied in the literature, and readers are referred to [24] and [25], for example, for more details.

In (5), the OCV and internal resistance are SOC-dependent, which can be expressed as follows:

$$V^o_{i,j}(k) = f_{i,j}\left(\mathrm{SOC}_{i,j}(k)\right) \tag{6a}$$

$$r_{i,j}(k) = h_{i,j}\left(\mathrm{SOC}_{i,j}(k)\right) \tag{6b}$$

where $f_{i,j}(\cdot)$ and $h_{i,j}(\cdot)$ are the nonlinear functions. The cell imbalance phenomena in the RBP can be characterized by assigning different values to $\mathrm{SOC}_{i,j}$, $f_{i,j}(\cdot)$, and $h_{i,j}(\cdot)$ in (5) and (6) for each battery cell $B_{i,j}$. Note that (5) and (6) can also capture the dynamics of the RBP composed of heterogeneous cells, such as nickel-cobalt-manganese (NCM) batteries and lithium-iron-phosphate (LFP) batteries, which exhibit distinct OCV–SOC curves and resistances.

Remark 4: The battery cell model presented in (5) is a simplified representation that omits certain electrochemical phenomena, including double-layer effects, charge-transfer reactions, and diffusion in solid electrodes. It is adopted in the unified modeling framework primarily for demonstration purposes, without loss of generality. It is important to note that this model can be readily replaced by a more sophisticated model, such as the Thevenin model [26] or the nonlinear double-capacitor model [27].

B. Battery Bank Model

1) To Model Banks of RBPs in Topology 1: The equivalent circuit model for battery bank i in the RBP of Topology 1 is illustrated in Fig. 7. In this configuration, each cell is equipped with a cell-level switch characterized by a contact resistance r_{cs}.

For the cell electrically connected to the battery bank, i.e., $u^c_{i,j}(k) = 1$, the bank voltage V^b_i can be derived from the cell's voltage $V^c_{i,j}$ and current $I^c_{i,j}$ according to Kirchhoff's voltage law, resulting in

$$V^c_{i,j}(k) - r_{\mathrm{cs}} I^c_{i,j}(k) = V^b_i(k). \tag{7}$$

For the cell bypassed in bank i, where $u^c_{i,j}(k) = 0$, its current $I^c_{i,j}$ is 0, and its terminal voltage equals its OCV $V^o_{i,j}$, as described in (5b). According to Kirchhoff's current law, the total current at the bank level, I^b_i, is the sum of the currents from all individual cells within the bank i. This relationship accounts for both connected and bypassed cells. This analysis leads to the following formulations:

$$V^c_{i,j}(k) = \begin{cases} V^b_i(k) + r_{\mathrm{cs}} I^c_{i,j}(k), & u^c_{i,j}(k) = 1 \\ V^o_{i,j}(k), & u^c_{i,j}(k) = 0 \end{cases} \tag{8a}$$

$$I^c_{i,j}(k) = \begin{cases} I^c_{i,j}(k), & u^c_{i,j}(k) = 1 \\ 0, & u^c_{i,j}(k) = 0 \end{cases} \tag{8b}$$

$$I^b_i(k) = \sum_{j=1}^{m} I^c_{i,j}(k). \tag{8c}$$

where the bank voltage and total current are scalars, expressed as $V^b_i \in \mathbb{R}$ and $I^b_i \in \mathbb{R}$.

2) To Model Banks of RBPs in Topology 2 or 4: For the RBPs in Topology 2 or 4, all cells within bank i are always connected, i.e., $u^c_{i,j}(k) = 1$, as described in (4). The absence of cell-level switches results in zero contact resistance, i.e., $r_{\mathrm{cs}} = 0$. Consequently, the relationship between a bank and its internal cells with respect to current and voltage can be established based on Kirchhoff's current and voltage laws, respectively, leading to

$$V^c_{i,j}(k) = V^b_i(k) \tag{9a}$$

$$I^b_i(k) = \sum_{j=1}^{m} I^c_{i,j}(k). \tag{9b}$$

3) Unified Bank Model: To facilitate the model presentation in a matrix–vector form, we define the following vectors and matrix:

$$\begin{aligned} V^c_i &= \left[V^c_{i,1}, V^c_{i,2}, \ldots, V^c_{i,m}\right]^T \in \mathbb{R}^m \\ V^o_i &= \left[V^o_{i,1}, V^o_{i,2}, \ldots, V^o_{i,m}\right]^T \in \mathbb{R}^m \\ I^c_i &= \left[I^c_{i,1}, I^c_{i,2}, \ldots, I^c_{i,m}\right]^T \in \mathbb{R}^m \\ U^c_i &= \mathrm{diag}\left(u^c_{i,1}, u^c_{i,2}, \ldots, u^c_{i,m}\right) \in \mathbb{R}^{m\times m} \end{aligned}$$

where diag$(\cdot)$ represents the diagonal matrix. Using these definitions, (8b) can be expressed in matrix form as $I^c_i(k) = U^c_i(k) I^c_i(k)$. By combining (8) and (9), the vectorized cell voltage V^c_i and the bank current I^b_i can be expressed as

$$\begin{aligned} V^c_i(k) = U^c_i(k)\left(V^b_i(k)\,1_m + R_s I^c_i(k)\right) \\ + \left(\mathbf{I}_m - U^c_i(k)\right) V^o_i(k) \end{aligned} \tag{10a}$$

$$I^b_i(k) = 1^T_m U^c_i(k)\, I^c_i(k) \tag{10b}$$

with

$$R_s = \begin{cases} r_{\mathrm{cs}}, & \text{for Toplogy 1} \\ 0, & \text{for Toplogies 2 and 4} \end{cases}$$

where $\mathbf{I}_m$ is the identity matrix with dimensions of $m \times m$ and 1_m represents the column vector with m ones.

By combining (5) and (10), the mathematical models for battery bank i in the RBPs with Topology 1, 2, or 4 can be unified and presented as follows:

$$\mathrm{SOC}_i(k+1) = \mathrm{SOC}_i(k) - B_i I_i^c(k) \tag{11a}$$

$$U_i^c(k)\,1_m V_i^b(k) = U_i^c(k)\,V_i^o(k) - (R_i(k) + R_s\mathbf{I}_m)\,U_i^c(k)\,I_i^c(k) \tag{11b}$$

$$I_i^b(k) = 1_m^T U_i^c(k)\,I_i^c(k) \tag{11c}$$

where $\mathrm{SOC_i}$ denotes the vector of SOCs of all cells in bank i, and B_i and R_i are diagonal matrices, which are mathematically defined as follows:

$$\mathrm{SOC}_i = \left[\mathrm{SOC}_{i,1}, \mathrm{SOC}_{i,2}, \ldots, \mathrm{SOC}_{i,m}\right]^T \in \mathbb{R}^m$$
$$B_i = \mathrm{diag}\left(\frac{\eta T}{Q_{i,1}}, \frac{\eta T}{Q_{i,2}}, \ldots, \frac{\eta T}{Q_{i,m}}\right) \in \mathbb{R}^{m\times m}$$
$$R_i = \mathrm{diag}\left(r_{i,1}, r_{i,2}, \ldots, r_{i,m}\right) \in \mathbb{R}^{m\times m}.$$

Using (11b), we calculate the voltage values of all branches connected to the electrical circuit of bank i and compile them into the vector $U_i^c 1_m V_i^b$. This formulation allows for a unified representation of the voltage distribution within bank i, regardless of whether individual cells are connected or bypassed.

4) Unified Bank Model With Measurable Input: Due to the constraints of hardware costs and space, it is impractical to furnish each individual cell in battery banks with a dedicated current sensor. Instead, only the total current of the battery pack is typically measurable. Cell imbalance further complicates this issue, as the currents flowing through the m parallel-connected cells in each bank are not equal. In addition, these currents fluctuate as the associated cell-level switches change their operating state within the reconfigured battery pack, posing a significant challenge for the accurate acquisition of cell-level currents in the RBP. This variability, combined with cell imbalance and the lack of individual current sensors, poses significant challenges for accurately acquiring cell-level currents I_i^c. These challenges consequently hinder effective applications of the battery bank model described in (11).

To address these challenges, we propose a method to derive the currents of battery cells in parallel connection in the RBP. This approach aims to overcome the limitations imposed by the lack of individual current sensors and the dynamic nature of the RBP. The proposed method is as follows. We begin by defining $\mathbf{0}_m \in \mathbb{R}^{m\times m}$ as the zero matrix of dimension $m \times m$. Within (11b), since R_i is full rank and $R_s \geq 0$, the matrix $R_i + R_s\mathbf{I}_m$ is invertible. By multiplying $(R_i + R_s\mathbf{I}_m)^{-1}$ on both sides of (11b), the cell-level currents I_i^c can be calculated through

$$U_i^c(k)\,I_i^c(k) = (R_i(k) + R_s\mathbf{I}_m)^{-1} \cdot U_i^c(k)\left(V_i^o(k) - 1_m V_i^b(k)\right) \tag{12}$$

where $U_i^c(k)$ on the left-hand side of the equation can be eliminated due to $U_i^c(k)I_i^c(k) = I_i^c(k)$.

When $U_i^c(k) \neq \mathbf{0}_m$, $1_m^T(R_i(k) + R_s\mathbf{I}_m)^{-1}U_i^c(k)1_m$ is a nonzero scalar, ensuring invertibility. By defining an intermediate variable (vector) Φ as follows:

$$\Phi = \left(1_m^T (R_i + R_s\mathbf{I}_m)^{-1} U_i^c 1_m\right)^{-1}\left(1_m^T (R_i + R_s\mathbf{I}_m)^{-1}\right).$$

Then, the size of Φ is $1 \times m$. The key idea is to express the bank voltage V_i^b in terms of the bank-level current I_i^b rather than the cell-level currents I_i^c. To achieve this, we multiply both sides of (11b) by Φ

$$\Phi(k)\,U_i^c(k)\,1_m V_i^b(k) = \Phi(k)\,U_i^c(k)\,V_i^o(k) - \Phi(k)\,(R_i(k) + R_s\mathbf{I}_m)\,U_i^c(k)\,I_i^c(k). \tag{13}$$

From (13), two important relationships can be derived

$$\Phi(k)\,U_i^c(k)\,1_m = 1 \tag{14a}$$

$$\Phi(k)\,(R_i(k) + R_s\mathbf{I}_m)\,U_i^c(k)\,I_i^c(k) = \left(1_m^T (R_i + R_s\mathbf{I}_m)^{-1} U_i^c 1_m\right)^{-1} 1_m^T U_i^c(k)\,I_i^c(k). \tag{14b}$$

By substituting the results from (11c) and (14) into (13), we can derive an expression for the bank voltage V_i^b as follows:

$$V_i^b(k) = \Phi(k)\,U_i^c(k)\,V_i^o(k) - \left(1_m^T (R_i(k) + R_s\mathbf{I}_m)^{-1} U_i^c(k)\,1_m\right)^{-1} I_i^b(k) \tag{15}$$

where only the bank-level current I_i^b, cell-level OCV values V_i^o, cell-level operating states U_i^c, and model parameters are required. Equation (15) provides a practical method for calculating the bank voltage using quantities that are either directly measurable or can be estimated with reasonable accuracy. This approach overcomes the challenges associated with measuring individual cell currents in the RBP.

When $U_i^c(k) = \mathbf{0}_m$, a special condition arises in the battery bank model. This scenario represents the case where all battery cells in bank i are disconnected from the electrical circuit. In this scenario, all currents of these cells and the bank-level current are 0, leading to $I_i^b = 0$ and $I_i^c = 0_m$. Correspondingly, the bank operating state $u_i^b(k) = 0$. The general bank model derived in (15) does not apply in this case, as the matrix $(R_i(k) + R_s\mathbf{I}_m)^{-1}U_i^c(k)$ becomes a zero matrix, leading to potential mathematical singularities.

For the bank i connected in the electrical circuit, its bank-level current I_i^b equals the pack-level current I^p. When it is bypassed, $I_i^b = 0$. This relationship is formulated as follows:

$$I_i^b(k) = u_i^b(k)\,I^p(k). \tag{16}$$

By substituting (15) and (16) into (11a), the state equation for battery bank i can be rewritten as follows:

$$\mathrm{SOC}_i(k+1) = \mathrm{SOC}_i(k) - B_i G_i(\mathrm{SOC}_i(k), I^p(k)). \tag{17}$$

In (17), $G_i(\cdot)$ is essentially a function of $\mathrm{SOC_i}$ and I^p in the form of

$$G_i(\cdot) = (R_i + R_s\mathbf{I}_m)^{-1} U_i^c \left[V_i^o - \left(1_m^T (R_i + R_s\mathbf{I}_m)^{-1} \cdot U_i^c 1_m\right)^{-1}\left(1_m^T (R_i + R_s\mathbf{I}_m)^{-1} U_i^c V_i^o - u_i^b I^p\right) 1_m\right]$$

where the time index k is omitted from all variables for brevity. Note that the elements of V_i^o and R_s are dependent on SOC, as indicated by (6). This dependency introduces nonlinearity into the model. Moreover, the matrices U_i^c and u_i^b capture the dynamic reconfiguration of the battery pack at both cell and bank levels. Finally, to implement the unified bank model

obtained in (17), one only needs the initial SOC of battery cells $\mathrm{SOC}_i(0)$, measured pack-level current I^p, and model parameters including R_s, R_i, and the SOC–OCV relationship. This formulation provides a comprehensive framework for modeling the bank-level voltage in RBPs, accounting for cell imbalances, dynamic reconfiguration, and measurable inputs. It allows for practical implementation in BMSs by relying on readily available measurements and estimates.

C. Battery Pack Model

The terminal voltage of the battery pack, denoted by V^p, is determined by the number of nonbypassed battery banks among all the n banks and the contact resistances of actively connected switches within the electrical circuit. Based on Kirchhoff's voltage law, V^p can be calculated by

$$V^p(k) = 1_n^T U^b(k) V^b(k) - \alpha r_{\mathrm{bs}} I^p(k) \tag{18}$$

where $U^b = \mathrm{diag}(u_1^b, u_2^b, \ldots, u_n^b) \in \mathbb{R}^{n\times n}$, $V^b = [V_1^b, V_2^b, \ldots, V_n^b] \in \mathbb{R}^n$, and α represents the number of closed bank-level switches connected in series with the nonbypassed battery banks, which depends on the specific topology and can be calculated as follows:

$$\alpha = \begin{cases} n, & \text{for Toplogies 1 and 2} \\ \displaystyle\sum_{i=1}^{n}\sum_{p=1}^{3} S_{i,p}^b - \sum_{i=1}^{n} S_{i,2}^b S_{i,3}^b, & \text{for Toplogy 4.} \end{cases} \tag{19}$$

Remark 5: Within RBPs with Topology 1 or 2, each battery bank i is associated with two bank-level switches, $S_{i,1}^b$ and $S_{i,2}^b$. Regardless of the operating state of the battery bank, one of these switches is always ON while the other is OFF. Consequently, this setup results in the value of α being equal to the total number of banks in the battery pack, namely, $\alpha = n$ in (19) for Topologies 1 and 2.

Remark 6: Within RBPs with Topology 4, the number of closed bank-level switches can be calculated as follows:

$$\alpha_1 = \sum_{i=1}^{n}\sum_{p=1}^{3} S_{i,p}^b \tag{20}$$

where $S_{i,p}^b$ can be derived from battery operating states through (2) and (3). According to the setup in Section III-B3, when $S_{i,2}^b$ is ON, $S_{i,3}^b$ will also be ON (while $S_{i,1}^b$ is OFF). However, in such cases, only $S_{i,2}^b$ is series-connected with nonbypassed battery banks, and the contact resistance of $S_{i,3}^b$ should not be considered. Therefore, we exclude the redundant contribution of $S_{i,3}^b$ from α_1. This is achieved by subtracting $\sum_{i=1}^n S_{i,2}^b S_{i,3}^b$ from α_1. This adjustment is reflected in the calculation of α in (19) for Topology 4.

From (16), the vector of currents passing through all battery banks, denoted by $I^b = [I_1^b, I_2^b, \ldots, I_n^b]^T \in \mathbb{R}^n$, can be expressed in vector form as follows:

$$I^b(k) = U^b(k) 1_n I^p(k). \tag{21}$$

The currents of all individual cells in the RBP can be compiled into the vector $I^c = [(I_1^c)^T, (I_2^c)^T, \ldots, (I_n^c)^T]^T \in \mathbb{R}^{nm}$. Based on (12) and (21), the cell-level currents I^c and the pack voltage V^b can be calculated as follows:

$$\begin{aligned} I^c(k) &= U^c(k)\left[R(k) + R_s \mathbf{I}_{nm}\right]^{-1} \\ &\quad \cdot \left[V^o(k) - V^b(k) \otimes 1_m\right] \end{aligned} \tag{22a}$$

$$\begin{aligned} V^b(k) &= \left[C^T\left[R(k) + R_s\mathbf{I}_{nm}\right]^{-1} U^c(k) C\right]^{-1} \\ &\quad \cdot \left[C^T\left[R(k) + R_s\mathbf{I}_{nm}\right]^{-1} U^c(k) V^o(k) \right. \\ &\quad \left. - U^b(k) 1_n I^p(k)\right] \end{aligned} \tag{22b}$$

where $\otimes$ denotes the Kronecker product. The matrices C, U^c, R, and V^o are defined as follows:

$$\begin{aligned} C &= \mathbf{I}_n \otimes 1_m \in \mathbb{R}^{nm\times n} \\ U^c &= \mathrm{diag}\left(U_1^c, U_2^c, \ldots, U_n^c\right) \in \mathbb{R}^{nm\times nm} \\ R &= \mathrm{diag}\left(R_1, R_2, \ldots, R_n\right) \in \mathbb{R}^{nm\times nm} \\ V^o &= \left[\left(V_1^o\right)^T, \left(V_2^o\right)^T, \ldots, \left(V_n^o\right)^T\right]^T \in \mathbb{R}^{nm}. \end{aligned}$$

Here, matrix C maps bank-level quantities to cell-level quantities, with each column corresponding to a bank and with ones for all cells in that bank. U^c represents the operating states of all cells in the pack, with each U_i^c the diagonal matrix of cell operating states for bank i. R represents the internal resistances of all cells in the pack, with each R_i the diagonal matrix of cell internal resistances for bank i. V^o compiles the open-circuit voltages of all cells in the pack, and each V_i^o is the vector of open-circuit voltages for cells in bank i. Key features of these definitions.

1) *Modularity:* The block diagonal structure of U^c and R allows for easy updating of individual bank properties.
2) *Scalability:* These definitions can accommodate RBPs of varying sizes by adjusting n and m.
3) *Reconfiguration Handling:* U^c captures the dynamic reconfiguration at the cell level for the entire pack.

The objective of this work is to develop a unified mathematical model in state-space form that can accurately describe the behavior of RBPs across all considered topologies, including their embedded banks and cells. In this model, the state variable is represented by x and the output by $y = [y_1, \ldots, y_4]^T$. The model inputs comprise the pack-level current $\xi = I^p \in \mathbb{R}$, bank-level operating states U^b, and cell-level operating states U^c. We define

$$\begin{aligned} x &= \left[\mathrm{SOC}_1^T, \mathrm{SOC}_2^T, \ldots, \mathrm{SOC}_n^T\right]^T \in \mathbb{R}^{nm} \\ y_1 &= \left[\left(V_1^c\right)^T, \left(V_2^c\right)^T, \ldots, \left(V_n^c\right)^T\right]^T \in \mathbb{R}^{nm} \\ y_2 &= I^c \in \mathbb{R}^{nm} \\ y_3 &= V^b \in \mathbb{R}^n \\ y_4 &= V^p \in \mathbb{R}. \end{aligned}$$

With the above definitions, the unified state-space model for RBPs can be derived from (17), (18), and (22), resulting in

$$x(k+1) = x(k) - B(k) G(x(k), \xi(k)) \tag{23a}$$

$$y_1(k) = F(x(k)) - H(x(k)) G(x(k), \xi(k)) \tag{23b}$$

$$y_2(k) = G(x(k), \xi(k)) \tag{23c}$$

$$y_3(k) = D(x(k), \xi(k)) \tag{23d}$$

$$y_4(k) = 1_n^T U^b(k) D(x(k), \xi(k)) - \alpha r_{\mathrm{bs}} \xi(k) \tag{23e}$$

where the matrix B, functions $F(\cdot)$, $H(\cdot)$, $G(\cdot)$, and $D(\cdot)$ are given by

$$\begin{aligned}
B &= \operatorname{diag}\left(B_1, B_2 \ldots B_n\right) \\
F(x) &= \left[f_{1,1}\left(\mathrm{SOC}_{1,1}\right), \ldots, f_{1,m}\left(\mathrm{SOC}_{1,m}\right)\right. \\
&\quad \left. \ldots, f_{n,1}\left(\mathrm{SOC}_{n,1}\right), \ldots, f_{n,m}\left(\mathrm{SOC}_{n,m}\right)\right]^T \\
H(x) &= \operatorname{diag}\left(h_{1,1}\left(\mathrm{SOC}_{1,1}\right), \ldots, h_{1,m}\left(SOC_{1,m}\right)\right. \\
&\quad \left. \ldots, h_{n,1}\left(\mathrm{SOC}_{n,1}\right), \ldots, h_{n,m}\left(\mathrm{SOC}_{n,m}\right)\right) \\
G(x,\xi) &= \left(H(x) + R_s \mathbf{I}_{nm}\right)^{-1} U^c \left(F(x) - D(x,\xi) \otimes 1_m\right) \\
D(x,\xi) &= \left(C^T \left(H(x) + R_s \mathbf{I}_{nm}\right)^{-1} U^c C\right)^{-1} \\
&\quad \cdot \left(C^T \left(H(x) + R_s \mathbf{I}_{nm}\right)^{-1} U^c F(x) - U^b 1_n \xi\right).
\end{aligned}$$

It is worth mentioning that U^c always equals $\mathbf{I}_{nm}$ for RBPs with Topology 2 or 4, regardless of the inputs, since they have no cell-level switches.

Remark 7: The unified state-space model for RBPs, presented in (23), demonstrates significant flexibility and extensibility, particularly in accommodating more complex cell models. The state variables in the present formulation encompass the SOC of all individual cells within the RBP system. If a higher order cell model is applied, as noted in Remark 4, this system's model can be seamlessly augmented. Such an augmentation would enhance the model's ability to capture more nuanced cell dynamics. In this scenario, while certain model components, such as the involved state variables and the output y_1, need to be updated, the fundamental structure of the unified state-space modeling framework will remain unchanged. The extended model could better address scenarios where detailed cell dynamics play a crucial role, such as in high-performance or safety-critical applications.

Remark 8: The pack-level current ξ in the unified state-space model (23) plays a crucial role in the system dynamics. During discharge, ξ is primarily determined by the applied load. During charging, ξ is influenced by the characteristics of the employed battery charger. When the design objective is to optimize or control battery configurations, as represented by U^b and U^c, under a given profile of ξ, it becomes advantageous to treat ξ as a disturbance in the model (23). The focus thereby shifts to designing robust control strategies for U^b and U^c that can accommodate variations in ξ. Moreover, the optimization problem can be formulated to find optimal configurations that perform well across a range of expected ξ profiles. In addition, it allows for a clear distinction between the controllable aspects (configuration) and the uncontrollable aspects (load demand) of the system. Furthermore, it encourages the development of configuration strategies that are resilient to variations in load profiles. Finally, it aligns with real-world scenarios where load demands may be uncertain or variable.

Remark 9: Due to its concise mathematical structure, the unified RBP model (23) can serve as an efficient and powerful tool for rapidly simulating and predicting the SOC, terminal voltages, and currents of all individual cells and banks within the RBP system. This model can accommodate RBPs with any number of series-connected banks and parallel-connected cells in a bank. Moreover, it may be extendable to topologies beyond those depicted in Fig. 1, suggesting broader applications in diverse battery system designs. These features significantly facilitate and simplify the analysis, optimization, and management of RBPs. In addition, the proposed model can also simulate the dynamics of battery packs with a fixed configuration by setting U^b and U^c as the identity matrices, and R_s and r_{bs} to zeros.

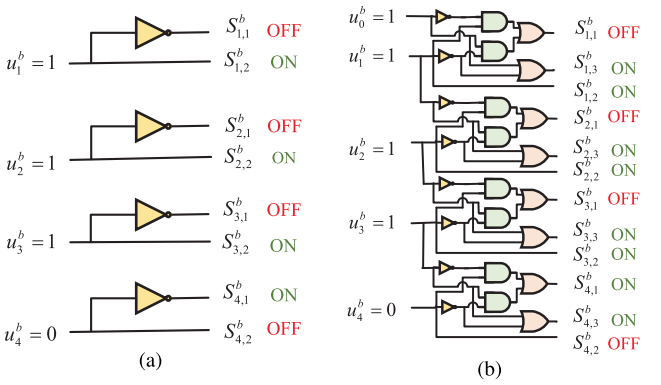

Fig. 8. For given operating states of battery banks, the derived operating states of bank-level switches using logic gate-based mappings. (a) RBPs with Topologies 1 and 2. (b) RBP with Topology 4.

Remark 10: The developed state-space model (23) facilitates the design of various model-based control strategies for RBPs. For instance, based on (23), a nonlinear model predictive control (NMPC) algorithm can be designed as follows to minimize the SOC variations among battery cells while satisfying voltage and current constraints

$$\begin{aligned}
&\min_{\substack{U^b(k), \ldots, U^b(k+N-1), \\ U^c(k), \ldots, U^c(k+N-1)}} J(x(k)) \\
&\text{s.t. } \forall i \in \{0, 1, \ldots, N-1\} \\
&\quad x(k+1) = x(k) - B(k) G(x(k), \xi(k)) \\
&\quad V_m^c 1_{nm} \le F(x(k)) - H(x(k)) \\
&\qquad \times G(x(k), \xi(k)) \le V_M^c 1_{nm} \\
&\quad I_m^c 1_{nm} \le G(x(k), \xi(k)) \le I_M^c 1_{nm}
\end{aligned} \tag{24}$$

with

$$\begin{aligned}
J(x(k)) &= \|x(k+N) - \bar{x}(k+N)\|_Q^2 \\
&\quad + \sum_{i=0}^{N-1} \left(\|x(k+i) - \bar{x}(k+i)\|_Q^2 \right. \\
&\quad \left. + \left\| U^b(k+i) \right\|_{R_1}^2 + \|U^c(k+i)\|_{R_2}^2 \right)
\end{aligned}$$

where V_m^c and V_M^c denote the minimum and maximum allowed cell voltage, and I_m^c and I_M^c are the minimum and maximum allowed cell current, respectively. The notation $\|x\|_Q^2$ represents $x^T Q x$, N is the prediction horizon, and Q, R_1, and R_2 are the corresponding positive weighting matrices.

V. Simulation Results and Discussion

To evaluate the developed unified modeling framework, which includes battery models at cell, bank, and pack levels,

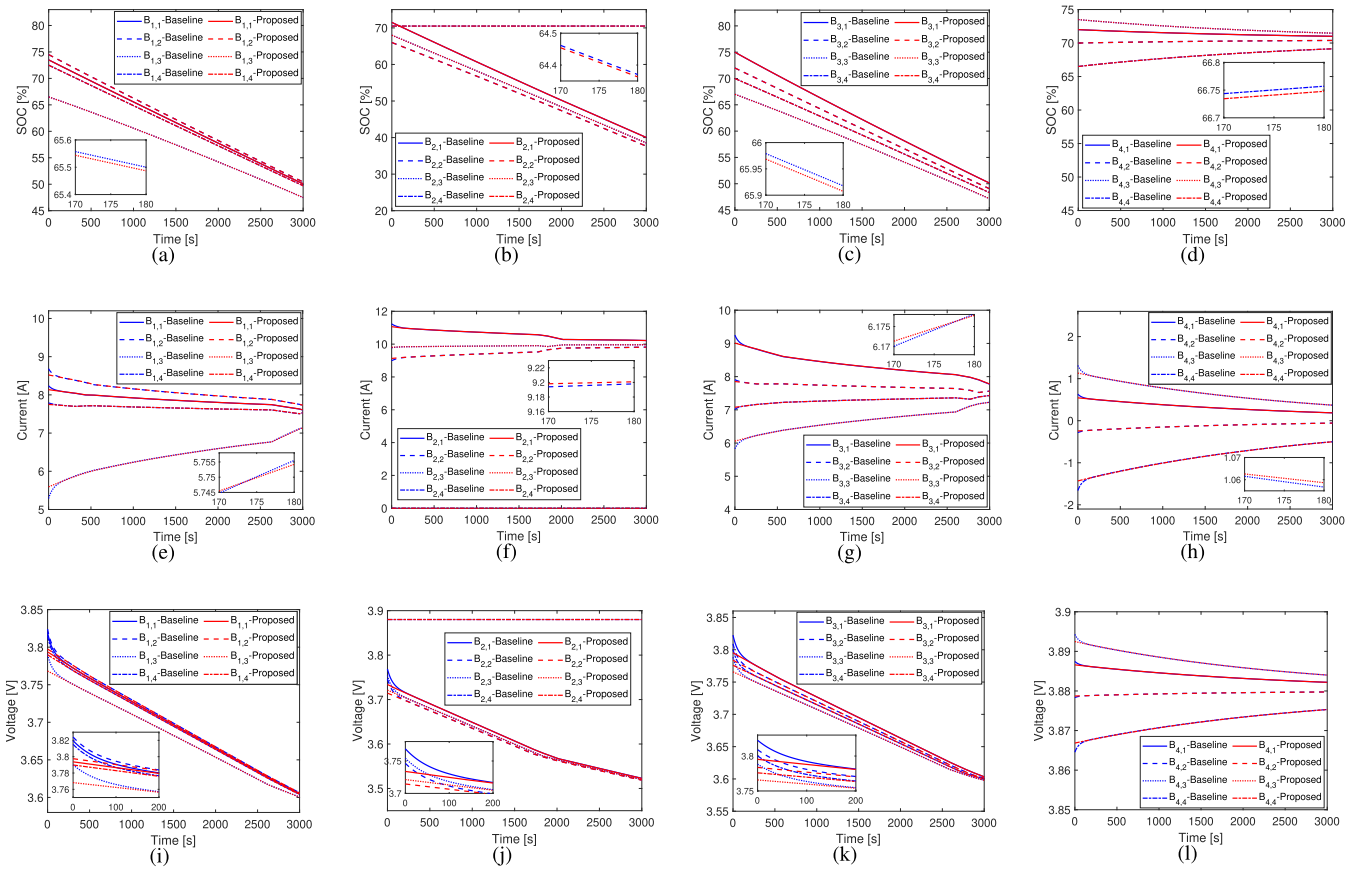

Fig. 9. Comparison of the proposed model against the ground truth (baseline) for RBPs with Topology 1. (a)–(d) Cell SOCs. (e)–(h) Cell-level currents. (i)–(l) Cell-level voltage.

extensive simulations are conducted using MATLAB R2022b on a 1.70-GHz Intel i5-10310U CPU. The simulation setup features a battery pack consisting of four battery banks connected in series, with each bank comprising four cells connected in parallel. The battery pack size is intentionally kept small to expedite model-based simulations and simplify the presentation of results. However, as noted in Remark 9, these numbers can be readily scaled up to meet the power and energy requirements of real-world battery systems. The nominal capacity of these cells is 28 A·h, and the ambient temperature for the tests is set to 20 °C. The initial SOC for different battery cells is randomly selected from the range of $[65\%, 75\%]$. The selected controllable switches for reconfiguration have a contact resistance of 0.01 Ω and an open conductance of 10^{-8} S. Sections V-A–V-C will present results from various simulation scenarios, focusing on aspects such as SOC evolution, voltage and current distributions, and the impact of different reconfiguration strategies. Performance metrics, including computational time and prediction accuracy, will be evaluated to demonstrate the efficacy of the unified modeling framework.

Accurately simulating a fixed-configuration battery pack and its cell-level dynamics presents significant challenges. These challenges are further amplified for dynamically RBPs. To comprehensively examine the accuracy and efficiency of the control-oriented model in (23), the Simscape simulator in the Simulink environment serves as a test bed. This simulator incorporating an embedded battery model is built on a set of blocks and has been experimentally validated against real-world batteries. In the Simscape model of the specified RBP, to describe the dynamics of battery cells, the battery cell model in (5) is extended to include a resistor–capacitor (RC) equivalent circuit. Parameters for this benchmark model, including cell OCV, series resistance, network resistance, and network capacitance, are sourced from the Simulink Library [28].

In the developed control-oriented RBP model (23), the internal resistance of battery cells, namely, $r_{i,j} = h_{i,j}(\cdot)$, is calculated as the sum of the series resistance and the network resistance. These parameter values are derived from the benchmark model in Simscape. The network capacitor is omitted in this formulation to simplify the model while maintaining sufficient accuracy for control purposes. The sampling period for the model is set to 1 s.

A. Results for RBPs With Uniform Cell Parameters

We first assess the accuracy of the proposed model (23) under conditions where all battery cells in the RBP have uniform model parameters, equal to their nominal value. Such conditions typically occur in the early stages of a battery pack's life.

For demonstration purposes, we consider the following scenario: the RBPs operate under a constant pack-level current

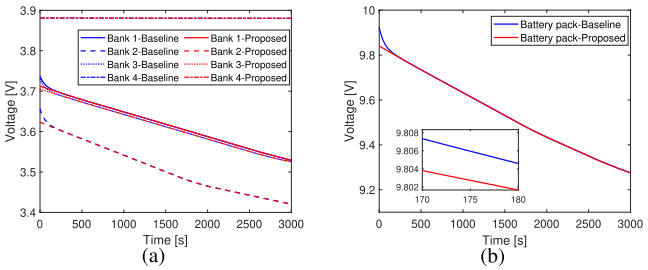

Fig. 10. Validation of the proposed model for reproducing terminal voltages in the RBP with Topology 1. (a) Bank-level voltages. (b) Pack voltage.

of 30 A, with battery bank 4 and cell $B_{2,4}$ bypassed. The corresponding operating states are given by

$$U^b = \mathrm{diag}\,(1,1,1,0)$$
$$U^c = \mathrm{diag}\,(1,1,1,1,1,1,1,0,1,1,1,1,1,1,1,1)\,.$$

In accordance with the above battery operating states, the operating states of bank-level switches for the RBPs with Topologies 1, 2, and 4 are derived utilizing the logic gate-based mappings established in Section III-B. The results are illustrated in Fig. 8. For the RBPs with Topology 1, all cell-level switches are ON, except $S^c_{2,4}$, which is OFF. In the RBPs with Topologies 2 and 4, there are no cell-level switches. Consequently, U^c is set to $\mathbf{I}_{16}$.

1) For the RBP With Topology 1: The SOC, current, and voltage of individual battery cells simulated by our model in (23) are compared with those from the Simspace simulator, which serve as the ground truth. The comparison results are presented in Fig. 9. Although its simpler structure and much fewer state variables, our model yields signal trajectories that closely match those of the benchmark. This high degree of consistency corroborates the validity of the proposed modeling framework and its internal models across different levels.

From Fig. 9(e)–(h), the currents of parallel-connected cells differ due to inconsistencies in their SOC values. Even if the battery bank is bypassed, mutual currents persist among its parallel-connected cells. Furthermore, voltages of these cells within the same bank vary due to nonuniform contact resistances of cell-level switches. These characteristics are accurately captured by our model, which further verifies its effectiveness.

In addition, the voltages of battery banks and the battery pack predicted by the proposed model are compared with their ground truth. As shown in Fig. 10, the proposed model is able to quickly converge to its benchmark, resulting in negligibly small steady-state modeling errors.

2) For the RBP With Topology 2 or 4: The voltage profiles of battery cells within each battery bank in Topology 2 are illustrated in Fig. 11. Again, a high level of consistency is achieved between the results of our mathematical model and the Simscape simulator. Unlike in Topology 1, the parallel-connected cells within the same bank in Topology 2 display identical voltage values. This observation aligns with our expectations, considering the absence of cell-level switches in Topology 2.

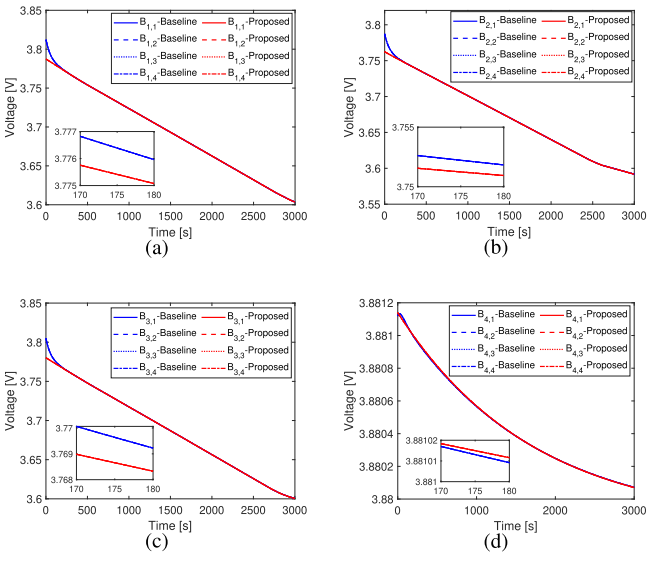

Fig. 11. Comparison of battery cell voltages simulated by the proposed model against its ground truth for the RBP with Topology 2. (a)–(d) Depict the results for four different banks, respectively.

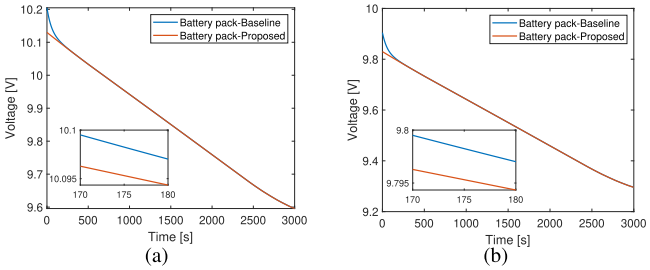

Fig. 12. Simulation results of pack voltages for (a) RBP with Topology 2 and (b) RBP with Topology 4.

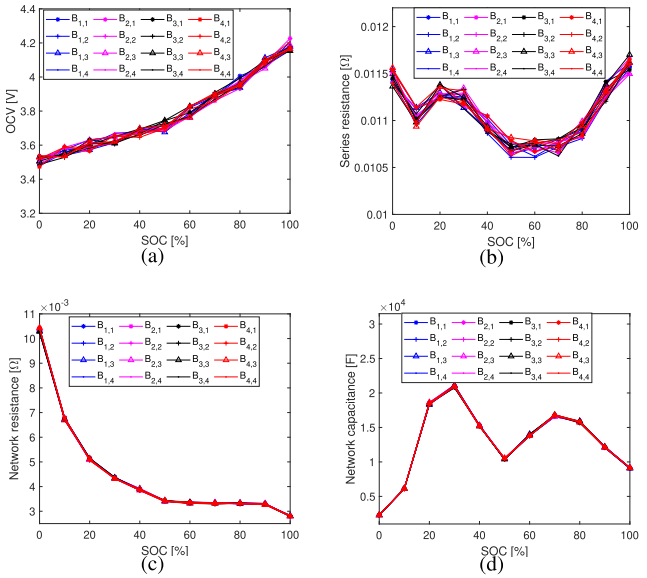

Fig. 13. Battery cell parameters and their dependencies on the SOC in the Simspace model. (a) OCV. (b) Series resistance. (c) Network resistance. (d) Network capacitance.

The pack voltage profiles of different topologies are investigated. By comparing Topology 1 in Fig. 10(b) with Topology 2 in Fig. 12, it is observed that the pack voltages differ for

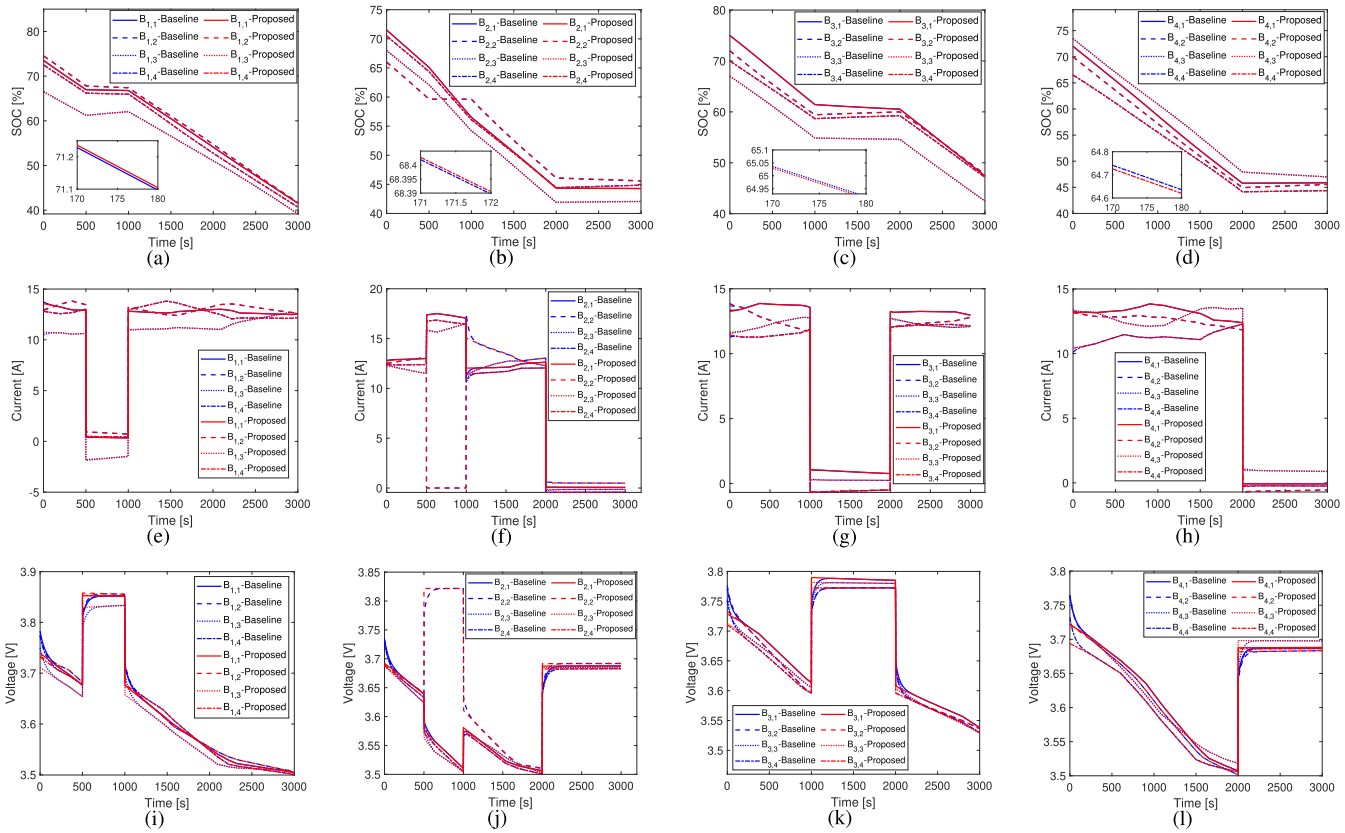

Fig. 14. Simulation results of (a)–(d) SOCs, (e)–(h) currents, (i)–(l) voltages of battery cells for RBP with Topology 1 based on the unified mathematical model (23) and Simscape block-based model.

RBPs with different topologies. Specifically, although the same battery cells are installed for all three RBPs, the RBP with Topology 2 exhibits the highest pack voltage during discharge. This is because, compared to the other two topologies, Topology 2 has fewer closed switches connected in series with the active battery banks and cells, resulting in a lower voltage drop caused by the contact resistance of the switches.

B. Results for RBPs With Inconsistent Cell Parameters

Due to manufacturing variations and nonuniform operating conditions, the cells in a battery pack are intrinsically heterogeneous. In addition to the ideal scenario considered in Section V-A, we further evaluate RBP models from the developed unified modeling framework, taking into account the inconsistencies in cell parameters. Fig. 13 depicts the nominal parameter values used for battery simulation in Simscape. Using these nominal values as the mean, we assume cell parameters in real-world applications follow a random distribution with a variance of 2%.

To operate the RBP system, the pack-level current I^p is specified as $I^p(t) = 50$ A. The other two model inputs, i.e., the bank-level operating states U^b and cell-level operating states U^c are defined as follows.

1) During $(0, 500$ s], no battery bank or cell is bypassed.
2) During $(500, 1000$ s], bank 1 and cell $B_{2,2}$ are bypassed.
3) During $(1000, 2000$ s], bank 3 is bypassed.
4) During $(2000, 3000$ s], banks 2 and 4 are bypassed.

For the RBP with Topology 1, as illustrated in Fig. 14, the battery states and outputs reproduced by (23) exhibit a high degree of similarity to those obtained from the baseline model, corroborating our model's accuracy. Specifically, when battery bank 1 is isolated during the time interval $(500, 1000$ s], as shown in 14(e), there are still interaction currents among its battery cells due to cell-to-cell inconsistencies, rather than all currents being 0. This shows that battery behaviors can be accurately simulated using the proposed model when the RBP is dynamically reconfigured. The evolution profiles of the pack voltage for RBPs with Topologies 1, 2, and 4 are shown in Fig. 15. Similar to the scenario in Section V-A, variations in pack voltage across different topologies are observed, and the RBP with Topology 2 exhibits the highest voltage.

Tests are also conducted to evaluate the influence of the switch contact resistance on the RBP's voltage. In the proposed model, the contact resistance is set to 0.008, 0.009, 0.01, and 0.011 Ω, respectively. The pack voltage profiles for RBPs with Topologies 1 and 2 are shown in Fig. 16. The results demonstrate that higher contact resistance leads to a greater pack-level voltage drop.

To further validate the performance of the unified model, simulations are carried out on the RPB with Topology 1. The federal urban driving schedule (FUDS) test profile [26] is employed, with a maximum current of 50 A. The pack-level current profile is shown in Fig. 17(a). The comparison results between the proposed model (23) and the baseline model in terms of the cell-level SOCs and the pack-level voltage are

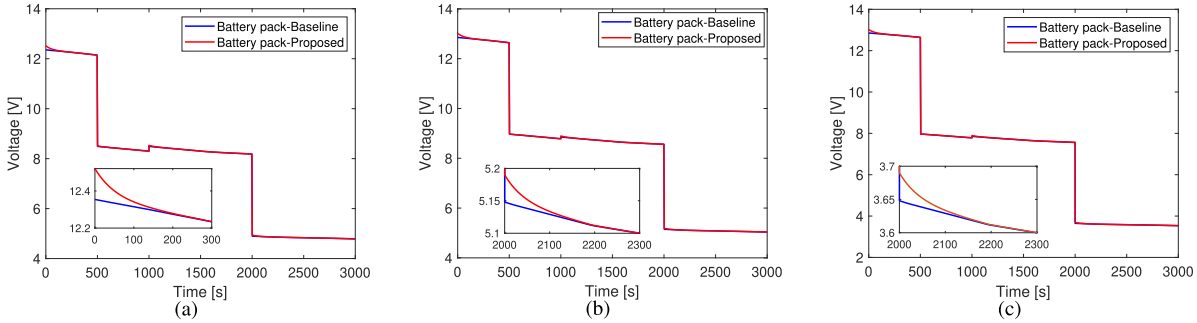

Fig. 15. Simulation results of pack voltages for (a) RBP with Topology 1, (b) RBP with Topology 2, and (c) RBP with Topology 4.

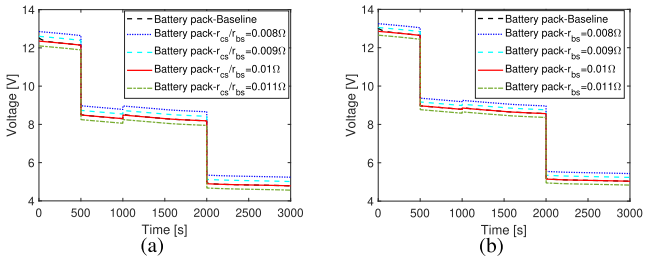

Fig. 16. Simulation results of the pack voltage for RBP with (a) Topologies 1 and (b) 2, with different switch contact resistance values.

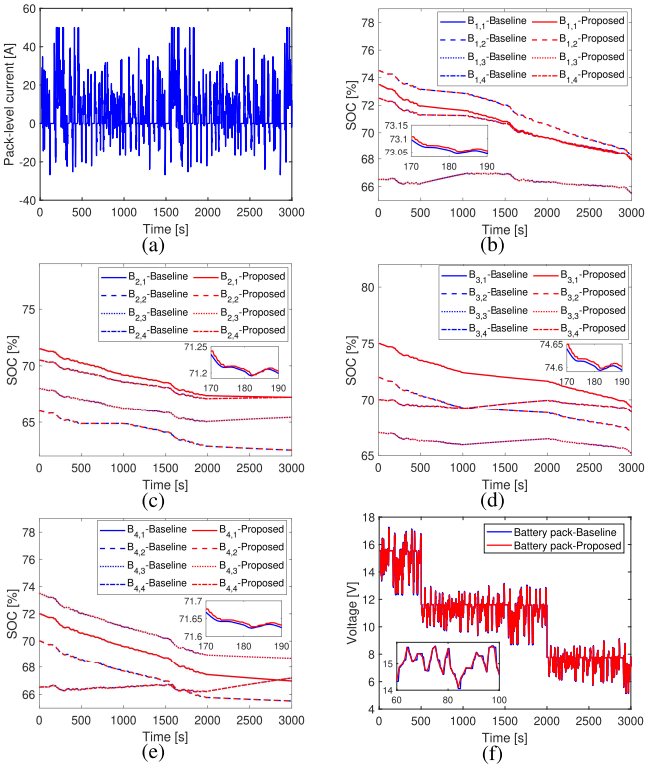

Fig. 17. Simulation results of (a) pack-level current, (b)–(e) cell SOCs, and (f) pack voltage for RBP with Topology 1 based on the unified model (23) and the Simscape block-based model.

presented in Fig. 17(b)–(f). The strong agreement between the two models demonstrates the proposed model's high accuracy.

C. Computational Efficiency Analysis

The practical implementation of RBP models in real-time management systems necessitates a careful evaluation of computational requirements. The results, as presented in Table I, demonstrate an average reduction of 47.12% in computational time compared to the Simscape simulator in Simulink. It should be pointed out that constructing or extending a model based on Simpscape blocks for RBPs needs good knowledge and experience in power electronics and is very time-consuming, especially for applications demanding high energy and power. This complexity primarily stems from the need to interconnect a large number of battery cell blocks with corresponding switch blocks and wires to simulate physical connections. In contrast, applying our mathematical model circumvents the complexity of physical block connections and significantly accelerates the RBP design process. In addition, the obtained state-space form enables the scalability of the model and facilitates the adjustment of dimensions m and n to adapt to larger scale battery packs, thereby substantially diminishing computational costs relative to the modeling approach based on the SimScape simulator. This computational efficiency is especially pronounced in the context of large-scale battery system modeling.

TABLE I
ELAPSED TIME COMPARISON OF THE PROPOSED MATHEMATICAL MODEL AND SIMSCAPE SIMULATOR

	RBP 1	RBP 2	RBP 4
Proposed model	2.9455 s	2.8638 s	2.9986 s
Simscape simulator	5.9534 s	5.2662 s	5.4728 s

To evaluate the proposed model when extended to large-scale RBP systems, simulations are conducted on an RBP with Topology 1, where $m = 6$ and $n = 10$. The battery bank 4 is bypassed. The results of cell SOCs, currents, and voltages are illustrated in Fig. 18.

Moreover, for battery management, fault prediction and diagnosis, state and parameter monitoring, optimization, and closed-loop control are indispensable. While striving for performance metrics, such as accuracy and optimality, it is crucial to ensure constraint satisfaction for safety. To this end, battery models are required as a fundamental tool to simulate and predict the dynamics of each RBP. This necessitates propagating the RBP model online, often multiple times within each time step, especially if iterative optimization methods or model-based predictive control are applied. Therefore, the computational efficiency is of utmost importance, particularly when hundreds of battery cells are contained in the pack. With

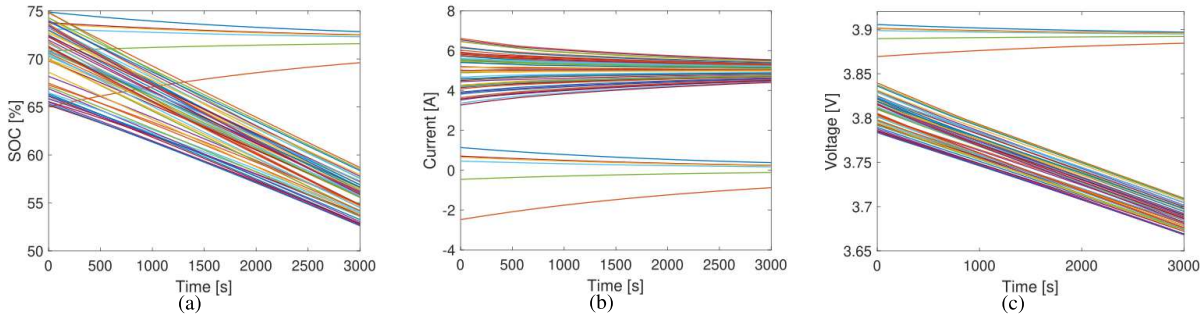

Fig. 18. Simulation results of (a) SOCs, (b) currents, and (c) voltages of the battery cells for RBP with Topology 1.

TABLE II
RELATIONSHIP BETWEEN OCV AND SOC OF THE BATTERY CELLS

SOC	0%	5%	10%	20%	30%	40%
OCV	2.5V	3.44V	3.502V	3.564V	3.636V	3.7V
SOC	50%	60%	70%	80%	90%	100%
OCV	3.774V	3.866V	3.952V	4.024V	4.08V	4.2V

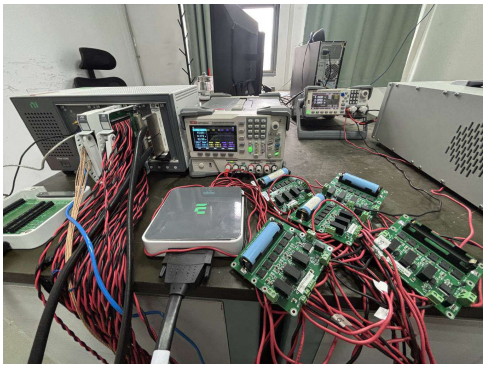

Fig. 19. Laboratory setup for RBP with Topology 1.

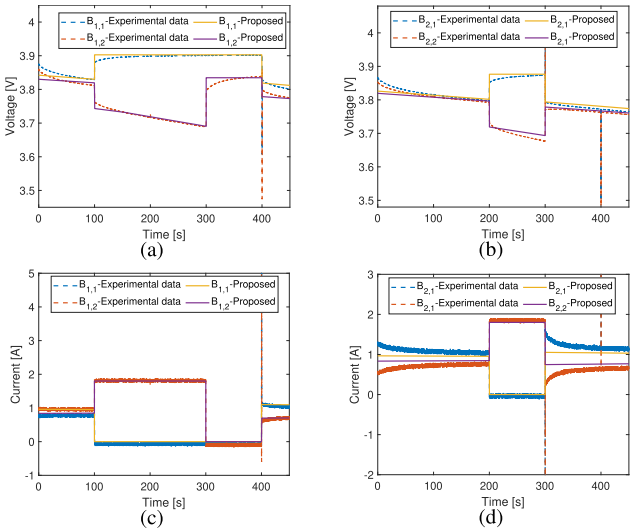

Fig. 20. Experimental data and simulation results from our proposed model (23). (a) and (b) Cell voltages. (c) and (d) Cell currents.

high computational efficiency, our proposed model lays a solid foundation for the online advanced management of RBPs that ensures both performance and safety.

VI. EXPERIMENTAL RESULTS

To test the performance of the proposed mathematical model, a laboratory prototype of the RBP with Topology 1 is built, as shown in Fig. 19. The RBP consists of two series-connected battery banks, each with two parallel-connected NCM 18650 1500-mA·h battery cells. The relationship between the cell OCV and SOC is seen in Table II. The cells' internal resistance are 0.0761, 0.0801, 0.0786, and 0.0809 Ω, and their initial SOCs are 65.74%, 62.80%, 64.19%, and 62.44%, respectively. The contact resistance of the MOSFETs is 0.05 Ω. The pack-level current is set as 1.8 A. The bank-level and cell-level reconfigurations are defined as follows.

1) During $(0, 100$ s], no battery bank or cell is bypassed.
2) During $(100, 200$ s], cell $B_{1,1}$ is bypassed.
3) During $(200, 300$ s], cells $B_{1,1}$ and $B_{2,1}$ are bypassed.
4) During $(300, 400$ s], cell $B_{1,1}$ and bank 1 are bypassed.
5) During $(400, 450$ s], no battery bank or cell is bypassed.

The simulation results from our model are compared with the experimental data in Fig. 20. As expected, and consistent with *Remark 4*, the system model using the one-state cell representation in (5) does not fully capture transient dynamics. However, it reliably reproduces the current and voltage profiles in steady and quasi-steady states. This corroborates the effectiveness of the proposed battery model.

Remark 11: As depicted in Fig. 20, transient current spikes lasting approximately 1–3 ms occur during configuration transitions due to the sequential nature of physical switch operations. These spikes are not intrinsic to reconfigurable battery technology but arise from specific hardware and control implementations. They can be mitigated by improving the coordination of switching signals, incorporating snubber capacitors to suppress current transients, and deploying fast-acting fuses as a final safeguard to interrupt unexpected surge currents. Note that the transient currents are not present in our model results.

VII. CONCLUSION

This work has, for the first time, developed a unified modeling framework for RBPs with various topologies. First, a set of logic gate-based mappings is developed to translate the

operations from batteries to switches. These mappings not only allow the RBP controller design to focus solely on batteries but also significantly reduce the number of control variables, the risk of false control coordination, and time delays in the operation of individual switches. Once the control policy is derived, it can be mapped to the control of switches at both the cell and bank levels. We then proceed with modeling from individual battery cells through banks and onward to packs, resulting in unified mathematical models capable of capturing their respective characteristics. This framework and its embedded models were validated under different scenarios and demonstrated high fidelity and computational efficiency.

The unified modeling framework features a state-space form and can accommodate RBPs with any number of series-connected banks and parallel-connected cells in a bank. This paves the way for a range of model-based analyses, optimization, and management of RBPs. In the future, we will experimentally validate models resulting from the developed framework under more diverse conditions and aging levels, and apply them in model-based optimization and control applications.

REFERENCES

[1] M. J. Brand, M. H. Hofmann, M. Steinhardt, S. F. Schuster, and A. Jossen, "Current distribution within parallel-connected battery cells," *J. Power Sources*, vol. 334, pp. 202–212, Dec. 2016.

[2] Y. Pan, X. Feng, M. Zhang, X. Han, L. Lu, and M. Ouyang, "Internal short circuit detection for Lithium-ion battery pack with parallel-series hybrid connections," *J. Cleaner Prod.*, vol. 255, May 2020, Art. no. 120277.

[3] Q. Ouyang, N. Ghaeminezhad, Y. Li, T. Wik, and C. Zou, "A unified model for active battery equalization systems," *IEEE Trans. Control Syst. Technol.*, vol. 33, no. 2, pp. 685–699, Mar. 2025.

[4] N. Ghaeminezhad, Q. Ouyang, X. Hu, G. Xu, and Z. Wang, "Active cell equalization topologies analysis for battery packs: A systematic review," *IEEE Trans. Power Electron.*, vol. 36, no. 8, pp. 9119–9135, Aug. 2021.

[5] J. Chen, Q. Ouyang, and Z. Wang, *Equalization Control for Lithium-Ion Batteries*. Singapore: Springer, 2023.

[6] W. Han, C. Zou, L. Zhang, Q. Ouyang, and T. Wik, "Near-fastest battery balancing by Cell/Module reconfiguration," *IEEE Trans. Smart Grid*, vol. 10, no. 6, pp. 6954–6964, Nov. 2019.

[7] Q. Ouyang, W. Han, C. Zou, G. Xu, and Z. Wang, "Cell balancing control for Lithium-ion battery packs: A hierarchical optimal approach," *IEEE Trans. Ind. Informat.*, vol. 16, no. 8, pp. 5065–5075, Aug. 2020.

[8] S. Ci, N. Lin, and D. Wu, "Reconfigurable battery techniques and systems: A survey," *IEEE Access*, vol. 4, pp. 1175–1189, 2016.

[9] A. Farakhor, D. Wu, Y. Wang, and H. Fang, "A novel modular, reconfigurable battery energy storage system: Design, control, and experimentation," *IEEE Trans. Transport. Electrific.*, vol. 9, no. 2, pp. 2878–2890, Jun. 2023.

[10] W. Han, T. Wik, A. Kersten, G. Dong, and C. Zou, "Next-generation battery management systems: Dynamic reconfiguration," *IEEE Ind. Electron. Mag.*, vol. 14, no. 4, pp. 20–31, Dec. 2020.

[11] A. Škegro, C. Zou, and T. Wik, "Analysis of potential lifetime extension through dynamic battery reconfiguration," in *Proc. 25th Eur. Conf. Power Electron. Appl. (EPE ECCE Eur.)*, Sep. 2023, pp. 1–11.

[12] T. Kim, W. Qiao, and L. Qu, "A series-connected self-reconfigurable multicell battery capable of safe and effective charging/discharging and balancing operations," in *Proc. 27th Annu. IEEE Appl. Power Electron. Conf. Expo. (APEC)*, Feb. 2012, pp. 2259–2264.

[13] L. He et al., "RAC: Reconfiguration-assisted charging in large-scale Lithium-ion battery systems," *IEEE Trans. Smart Grid*, vol. 7, no. 3, pp. 1420–1429, May 2016.

[14] X. Liu, G. Chang, J. Tian, Z. Wei, X. Zhang, and P. Wang, "Flexible path planning-based reconfiguration strategy for maximum capacity utilization of battery pack," *J. Energy Chem.*, vol. 86, pp. 362–372, Nov. 2023.

[15] H. Cui, Z. Wei, H. He, and J. Li, "Novel reconfigurable topology-enabled hierarchical equalization of Lithium-ion battery for maximum capacity utilization," *IEEE Trans. Ind. Electron.*, vol. 70, no. 1, pp. 396–406, Jan. 2023.

[16] H. Huang, A. M. Y. M. Ghias, P. Acuna, Z. Dong, J. Zhao, and M. S. Reza, "A fast battery balance method for a modular-reconfigurable battery energy storage system," *Appl. Energy*, vol. 356, Feb. 2024, Art. no. 122470.

[17] F. An, W. Zhang, B. Sun, J. Jiang, and X. Fan, "A novel battery pack inconsistency model and influence degree analysis of inconsistency on output energy," *Energy*, vol. 271, May 2023, Art. no. 127032.

[18] Q. Yu, Y. Huang, A. Tang, C. Wang, and W. Shen, "OCV-SOC-temperature relationship construction and state of charge estimation for a series–parallel Lithium-ion battery pack," *IEEE Trans. Intell. Transp. Syst.*, vol. 24, no. 6, pp. 6362–6371, Jun. 2023.

[19] J. Millman and C. Halkias, *Microelectronics: Digital and Analog Circuits and Systems*. New York, NY, USA: McGraw-Hill, 1979.

[20] A. Clements, *Principles of Computer Hardware*. London, U.K.: Oxford Univ. Press, 2006.

[21] C.-F. Juang, C.-M. Lu, C. Lo, and C.-Y. Wang, "Ant colony optimization algorithm for fuzzy controller design and its FPGA implementation," *IEEE Trans. Ind. Electron.*, vol. 55, no. 3, pp. 1453–1462, Mar. 2008.

[22] S.-Z. Chen, Y. Wang, G. Zhang, L. Chang, and Y. Zhang, "Sneak circuit theory based approach to avoiding short-circuit paths in reconfigurable battery systems," *IEEE Trans. Ind. Electron.*, vol. 68, no. 12, pp. 12353–12363, Dec. 2021.

[23] Q. Ouyang, Z. Wang, K. Liu, G. Xu, and Y. Li, "Optimal charging control for Lithium-ion battery packs: A distributed average tracking approach," *IEEE Trans. Ind. Informat.*, vol. 16, no. 5, pp. 3430–3438, May 2020.

[24] X. Lin et al., "A lumped-parameter electro-thermal model for cylindrical batteries," *J. Power Sources*, vol. 257, pp. 1–11, Jul. 2014.

[25] X. Hu, H. Yuan, C. Zou, Z. Li, and L. Zhang, "Co-estimation of state of charge and state of health for Lithium-ion batteries based on fractional-order calculus," *IEEE Trans. Veh. Technol.*, vol. 67, no. 11, pp. 10319–10329, Nov. 2018.

[26] H. He, R. Xiong, X. Zhang, F. Sun, and J. Fan, "State-of-charge estimation of the Lithium-ion battery using an adaptive extended Kalman filter based on an improved Thevenin model," *IEEE Trans. Veh. Technol.*, vol. 60, no. 4, pp. 1461–1469, May 2011.

[27] H. Movahedi, N. Tian, H. Fang, and R. Rajamani, "Hysteresis compensation and nonlinear observer design for state-of-charge estimation using a nonlinear double-capacitor Li-ion battery model," *IEEE/ASME Trans. Mechatronics*, vol. 27, no. 1, pp. 594–604, Feb. 2022.

[28] MathWorks. *Equivalent Circuit Battery*. [Online]. Available: https://ww2.mathworks.cn/help/autoblks/ref/equivalentcircuitbattery.html

Quan Ouyang (Member, IEEE) received the B.S. degree in automation from the Huazhong University of Science and Technology, Wuhan, China, in 2013, and the Ph.D. degree in control science and engineering from Zhejiang University, Hangzhou, China, in 2018.

He was a Post-Doctoral Researcher with the Department of Electrical Engineering, Chalmers University of Technology, Gothenburg, Sweden. He is currently an Associate Professor with the College of Automation Engineering, Nanjing University of Aeronautics and Astronautics, Nanjing, Jiangsu, China. His research interests mainly include battery management, modeling and control of fuel cell systems, and nonlinear control.

Albert Škegro (Student Member, IEEE) received the B.Sc. and M.Sc. degrees in electrical engineering from the University of Zagreb, Zagreb, Croatia, in 2016 and 2018, respectively. He is currently pursuing the Ph.D. degree in automatic control with the Department of Electrical Engineering, Chalmers University of Technology, Gothenburg, Sweden.

From 2016 to 2017, he studied as an Erasmus Exchange Student at Karlsruhe Institute of Technology, Karlsruhe, Germany. From 2018 to 2020, he was a Battery Control Engineer with Rimac Automobili Ltd., Sveta Nedelja, Croatia. His research interests include battery modeling, control, optimization, and predictive maintenance in electric powertrains.

Mr. Škegro has received several distinctions, including the Special Dean Award from the University of Zagreb, fellowships from DAAD and French Ministry of National Education, and Second Place in the 2025 IEEE Vehicular Technology Society Call for Ideas Competition for work on reconfigurable battery systems.

Lin Hu (Member, IEEE) received the Ph.D. degree in engineering from the School of Mechanical and Automotive Engineering, Hunan University, Changsha, China, in 2008.

From 2009 to 2011, he was a Post-Doctoral Researcher with the University of Hannover, Hannover, Germany. Since 2011, he has been with the School of Automotive and Mechanical Engineering, Changsha University of Science and Technology, Changsha, where he is currently a Professor. His research interests include intelligent vehicles, traffic safety, and vehicle energy management.

Dr. Hu is a fellow of China Society of Automotive Engineers and serves as a Standing Council Member of Chinese Society for Construction Machinery and a Council Member of China Society of Automotive Engineers. He was a recipient of the National Science Fund for Distinguished Young Scholars of China and Hunan Provincial Distinguished Young Scholar Fund, and he was selected as a Hunan "Furong Scholar." He has served as an Expert Reviewer for the National Key Research and Development Program, the Ministry of Education Talent Programs, the National Natural Science Foundation of China, and provincial and ministerial projects. He is an Associate Editor of *Chinese Journal of Mechanical Engineering* (English Edition) and *China Journal of Highway and Transport*, and on the Editorial Board of *Sustainability*.

Weiji Han (Member, IEEE) received the Ph.D. degree in electrical engineering from the University of Connecticut, Storrs, CT, USA, in 2018.

He was a Post-Doctoral Researcher and then a Researcher with Chalmers University of Technology, Gothenburg, Sweden, from 2018 to 2021. Since 2022, he has been an Associate Professor with China-UK Low Carbon College, Shanghai Jiao Tong University, Shanghai, China. He has led collaborative projects between Sweden and the National Natural Science Foundation of China, as well as Shanghai International Science and Technology Cooperation Projects, and has participated in six research projects funded by U.S. Department of Energy and the Swedish Ministry of Energy. His research focuses on modeling, analysis, control, and optimization of battery energy storage systems, with applications in smart grids and electric vehicles.

Dr. Han was a recipient of the Marie Skłodowska-Curie Fellowship and Shanghai Leading Talent (Overseas) Award. He is currently serving as an Associate Editor for *IET Generation, Transmission and Distribution* and a Guest Editor for *Batteries*.

Dezhi Ren (Student Member, IEEE) received the B.E. degree in electronic information engineering from Harbin Institute of Technology, Weihai, China, in 2023. He is currently pursuing the M.E. degree in energy and power engineering with Shanghai Jiao Tong University, Shanghai, China.

His research interests primarily focus on embedded system development, with recent work emphasizing the exploration of reconfigurable battery systems and automotive electronics.

Changyou Geng (Graduate Student Member, IEEE) received the B.E. degree in energy and power engineering from Hohai University, Nanjing, China, in 2018, and the M.E. degree in power engineering from Tianjin University, Tianjin, China, in 2021. He is currently pursuing the D.Eng. degree in energy and power engineering with Shanghai Jiao Tong University, Shanghai, China.

His research interests include battery management systems, optimal control algorithms, and reconfigurable battery systems.

Torsten Wik (Senior Member, IEEE) received the M.Sc. degree in chemical engineering (major in applied mathematics), the Licentiate of Engineering degree in control engineering, the Ph.D. degree in environmental sciences (major in automatic control), and the Docent degree in electrical engineering from the Chalmers University of Technology, Gothenburg, Sweden, in 1994, 1996, 1999, and 2004, respectively.

He is a Professor and the Head of the Automatic Control Group, Department of Electrical Engineering, Chalmers University of Technology. His current research interests include optimal control, model reduction, and systems with model uncertainties, with applications to energy storage, environmental, and biological systems.

Changfu Zou (Senior Member, IEEE) received the Ph.D. degree in automation and control engineering from the University of Melbourne, Melbourne, VIC, Australia, in 2017.

He was a Visiting Student Researcher with the University of California at Berkeley, Berkeley, CA, USA, from 2015 to 2016. Since early 2017, he has been with the Automatic Control Unit, Chalmers University of Technology, Gothenburg, Sweden, where he started as a Post-Doctoral Researcher and then became an Assistant Professor and is currently an Associate Professor. His research focuses on advanced modeling and automatic control of energy storage systems, particularly batteries.

Dr. Zou received several prestigious grants from European Commission and Swedish national agencies and has hosted five researchers to achieve the Marie Skłodowska-Curie Fellows. He serves as an Associate Editor/Editorial Board Member for journals, such as IEEE TRANSACTIONS ON VEHICULAR TECHNOLOGY, IEEE TRANSACTIONS ON TRANSPORTATION ELECTRIFICATION, and *iScience* (Cell Press).